AD-A087 255 LOCKHEED MISSILES AND SPACE CO INC PALO ALTO CA PALO --ETC F/G 20/14
STUDY OF ELF PROPAGATION ANOMALIES AS RELATED TO IMPROVED KNOWL--ETC(U)
JAN 80 W L IMHOF, R C GUNTON, T R LARSEN N00014-79-C-0175
UNCLASSIFIED LMSC/D681778 NL

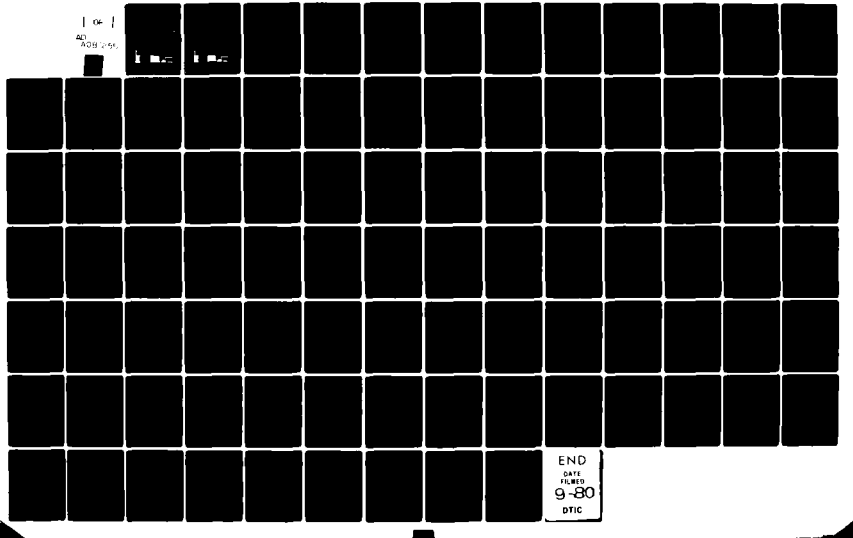

END
DATE FILMED
9-80
DTIC

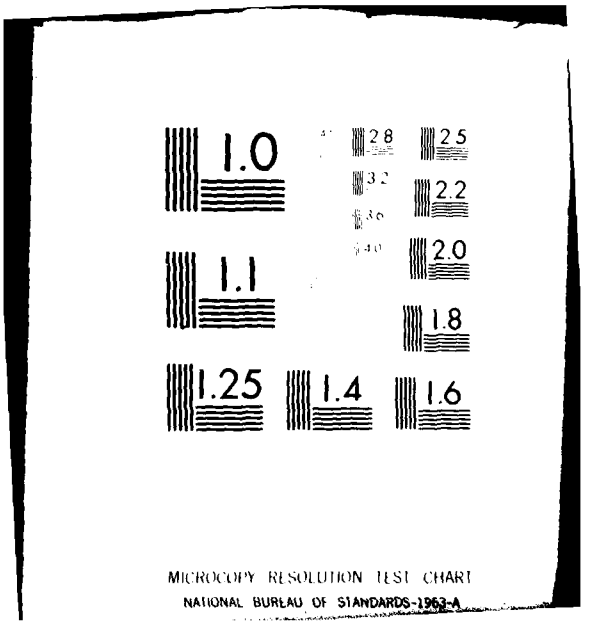
1.0
2.8
2.5
3.2
2.2
3.6
4.0
2.0
1.1
1.8
1.25
1.4
1.6
MICROCOPY RESOLUTION TEST CHART
NATIONAL BUREAU OF STANDARDS-1963-A

LEVEL II

TASK NO. NR 089-142
LMSC-D681778
30 JANUARY 1980

The research was sponsored by the Office of Naval Research
Contract N00014-79-C-0175, Task No. NR 089-142

STUDY OF ELF PROPAGATION ANOMALIES AS RELATED TO IMPROVED KNOWLEDGE OF ELECTRON DENSITY PROFILES PRODUCED BY ENERGETIC PARTICLE PRECIPITATION

ANNUAL TECHNICAL REPORT

Contract Number N00014-79-C-0175

W. L. Imhof
R. C. Gunton
T. R. Larsen
E. E. Gaines
J. B. Reagan
R. E. Meyerott

LOCKHEED
PALO ALTO RESEARCH LABORATORY
LOCKHEED MISSILES & SPACE COMPANY, INC • A SUBSIDIARY OF LOCKHEED AIRCRAFT CORPORATION
PALO ALTO, CALIFORNIA

TASK NO. NR 089-142
LMSC-D681778
30 JANUARY 1980

The research was sponsored by the Office of Naval Research
Contract N00014-79-C-0175, Task No. NR 089-142

STUDY OF ELF PROPAGATION ANOMALIES AS RELATED TO IMPROVED KNOWLEDGE OF ELECTRON DENSITY PROFILES PRODUCED BY ENERGETIC PARTICLE PRECIPITATION

ANNUAL TECHNICAL REPORT

Contract Number N00014-79-C-0175

W. L. Imhof
R. C. Gunton
T. R. Larsen
E. E. Gaines
J. B. Reagan
R. E. Meyerott

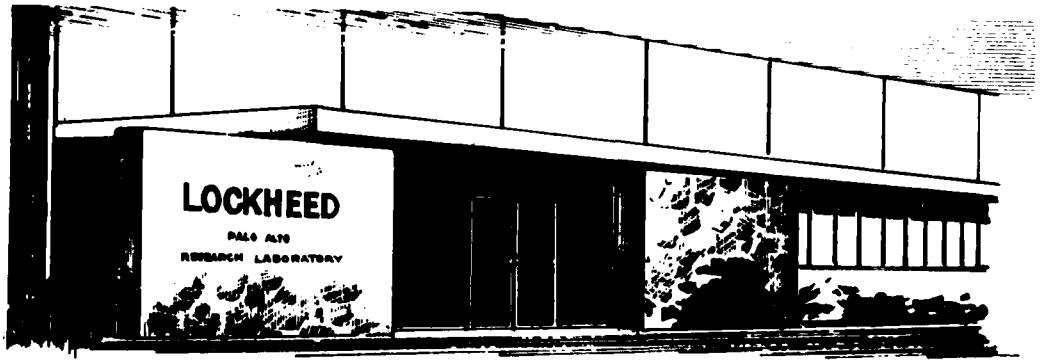

LOCKHEED

PALO ALTO RESEARCH LABORATORY

LOCKHEED MISSILES & SPACE COMPANY, INC. • A SUBSIDIARY OF LOCKHEED AIRCRAFT CORPORATION
PALO ALTO, CALIFORNIA

UNCLASSIFIED

SECURITY CLASSIFICATION OF THIS PAGE (When Data Entered)

REPORT DOCUMENTATION PAGE

READ INSTRUCTIONS BEFORE COMPLETING FORM

1. REPORT NUMBER: LMSC-D681778	2. GOVT ACCESSION NO.: AD-A087 255
3. RECIPIENT'S CATALOG NUMBER:	
4. TITLE (and Subtitle): STUDY OF ELF PROPAGATION ANOMALIES AS RELATED TO IMPROVED KNOWLEDGE OF ELECTRON DENSITY PROFILES PRODUCED BY ENERGETIC PARTICLE PRECIPITATION.	5. TYPE OF REPORT & PERIOD COVERED: Annual Technical Report, for period ending 30 Nov 79
	6. PERFORMING ORG. REPORT NUMBER: LMSC-D61778
7. AUTHOR(s): William L. Imhof, Robert C. Gunton, Trygve R. Larsen, Joseph B. Reagan, Edward E. Gaines, and Roland E. Meyerott.	8. CONTRACT OR GRANT NUMBER(s): N00014-79-C-0175
9. PERFORMING ORGANIZATION NAME AND ADDRESS: Space Sciences Laboratory, LOCKHEED PALO ALTO RESEARCH LABORATORY, 3251 Hanover Street, Palo Alto, CA 94304	10. PROGRAM ELEMENT, PROJECT, TASK AREA & WORK UNIT NUMBERS: NR 089-142
11. CONTROLLING OFFICE NAME AND ADDRESS: Department of the Navy, Office of Naval Research, Code 464, Arlington, VA 22217	12. REPORT DATE: 30 January 1980 13. NUMBER OF PAGES: 85
14. MONITORING AGENCY NAME & ADDRESS (if different from Controlling Office)	15. SECURITY CLASS. (of this report): UNCLASSIFIED 15a. DECLASSIFICATION/DOWNGRADING SCHEDULE

16. DISTRIBUTION STATEMENT (of this Report)

Approved for Public Release and Sale: Distribution Unlimited

17. DISTRIBUTION STATEMENT (of the abstract entered in Block 20, if different from Report)

18. SUPPLEMENTARY NOTES

19. KEY WORDS (Continue on reverse side if necessary and identify by block number)

ELF transmission anomalies	Free electron concentrations
Satellite energetic particle data	D-region electron densities
Precipitating electrons	Solar particle events
Ion-pair production rates	Polar cap absorption events

20. ABSTRACT (Continue on reverse side if necessary and identify by block number)

A study has been made of extremely low frequency (ELF) wave propagation anomalies as related to energetic particle precipitation, principally during solar particle events (SPE). Based on calculation of the predicted signal strengths at Tromso for transmissions from the Wisconsin Test Facility (WTF) a criterion has been selected for possible use in a field test operation. If the ion pair production rates at 40 km are equal to or greater than $1 \times 10^3 cm^{-3} sec^{-1}$ then it is probable that a 3 dB or larger reduction in signal strength would occur for such an event. Since this preliminary criterion is based on ELF signal strength computation

DD FORM 1 JAN 73 1473 EDITION OF 1 NOV 65 IS OBSOLETE

UNCLASSIFIED

SECURITY CLASSIFICATION OF THIS PAGE (When Data Entered)

20. (Abstract), continued

assuming no local time variations along the propagation path, more detailed calculations of the local time ionospheric effects should be performed.

Intercomparisons have been made of the calculations of ELF propagation over the WTF to Tramso path performed by three different laboratories; LMSC, Naval Ocean Systems Center (W. Moler) and Pacific Sierra Research (E. C. Field). The calculations were made using five daytime and nighttime test profiles of ion and electron densities provided by LMSC (J. B. Reagan). The results of the comparisons show a considerable measure of agreement but illustrate the importance of segmentation of the path and selection of ground conductivities.

A study was made of the expected effect of local time variations during solar particle events on the ELF propagation over the path from WTF to Tromso. Electron and ion density profiles for the various segments of the test path were calculated with the ion chemistry model, taking into account the local time for each segment. In a comparison of conditions measured and calculated for SPE72 on 4 August 1972 near the peak of the event and conditions calculated for a similar case assuming a season of 21 December, very little difference in signal strength attenuation over the path was found.

Improvements have been made in an existing LMSC ion chemistry model based on satellite particle precipitation measurements and radar electron density measurements performed during the intense solar particle event of 4 August 1972. The improvements are based on theoretical studies which indicate that in order to obtain correct electron densities the effects of negative ions must be taken into account. Accordingly, the densities for the August 1972 SPE have been revised and the required model revisions made with emphasis placed on using the available data at the lower altitudes 60 - 50 km, of greater importance for ELF propagation.

It is shown that sporadic E-layer effects can have a major effect on ELF propagation during a solar particle event. Since they occur at a reasonably high frequency, sporadic E-layers should be considered in planning an ELF-PCA field program.

TABLE OF CONTENTS

Section 1
INTRODUCTION

It is well established that the transmissions of extremely low frequency (ELF) waves at nighttime are subject to wide variations. At least some of the observed anomalies are known to be due to enhanced ionization caused by the precipitation of energetic electrons and protons into the earth's atmosphere (Davis, 1974, 1976; Davis and Meyers, 1975; Larsen, 1974a). A successful correlation between anomalous signal strengths and precipitating particles was established for the first time in 1976 (Imhof et al, 1976; Reagan et al, 1978a). This preliminary finding, based primarily on the measured transmisions between the Wisconsin Test Facility (WTF) and the mid-latitude receiving site in Connecticut and direct satellite measurements of precipitating particles, has formed a basis for further more quantitative studies of the cause-and-effect relationship.

Subsequent studies of the effects of energetic particle precipitation on ELF transmission signal strength have been made at the Lockheed Palo Alto Research Laboratory (LPARL) based partly on data acquired with scientific payloads on the low altitude polar orbiting satellites 1971-089A and 1972-076B developed by the Space Sciences Laboratory of LPARL for the Office of Naval Research, the Defense Nuclear Agency, and the Defense Advanced Research Projects Agency. In these investigations, supported by the Office of Naval Research, ELF propagation data were obtained from Dr. John Davis of the Naval Research Laboratory, Washington, D.C., and P. R. Bannister of Naval Underwater Systems Center, New London, Connecticut. This large data set includes measurements taken during coordinated exercises involving ELF transmission between the U. S. Navy Wisconsin Test Facility and receiving stations in Connecticut, Maryland, Greenland, Norway, and Italy performed in March - April 1975 and March - April 1976. These studies have provided further verification of the importance of particle precipitation. Since the details of the horizontal and vertical distributions of the enhanced ionization are clearly very important, a large body of coordinated data is required to

provide quantitative interpretations of the results and to assess the impact of important chemistry parameters on the transmitted ELF signal strength. Clearly, good chemistry models are also needed for a proper evaluation of the coordinated data. In this regard the satellite/Chatanika backscatter radar data acquired during the August 1972 solar particle event are particularly useful.

With the energetic particle data obtained from payloads on the low altitude polar-orbiting satellites 1971-089A and 1972-076B, in 1976 a qualitative correlation was established between anomalous ELF signal levels received at Connecticut and the precipitation of significant fluxes of electrons from the radiation belts. However, a detailed quantitative correlation between the sign (signal enhancement versus degradation) and severity of the anomalies and particle characteristics such as intensities and spectra was not firmly established because of the limited data base used. Stimulated by these findings, special coordinated exercises were conducted in March - April 1976 involving satellite measurements of the precipitating particles and ELF transmissions between the U. S. Navy Wisconsin Test Facility and receiving stations in Maryland, Greenland, Norway, and Italy. Coordinated satellite/ELF transmission measurements were also made in March - April 1975 and July 1975.

Detailed discussions of the investigations performed from the coordinated data sets acquired in 1975 and 1976 are provided in the previous annual reports (Imhof, et al., 1976, 1977) and by Reagan, et al. (1978a). Briefly, the following major conclusions have followed from these study efforts:

- From coordinated satellite and ELF attenuation measurements, it has been found that direct particle precipitation into the atmosphere can cause ELF transmission anomalies. In these anomalies the signal strengths may be either attenuated or enhanced depending upon the geometry and details of the ion and electron density profiles resulting from the particle precipitation.
- Sensitivity studies were made to assess the dependence of the ELF signal strengths on such parameters as the electron and ion density profiles and their distribution along the propagation path.

- o The signal strengths tend to decrease with increasing electron density at altitudes of 60 km or lower.
- o The effect of a given ionization profile depends strongly on its location.
- o The ELF signal strengths are most sensitive to positive ion density profiles at altitudes of 45 km or lower.
- o The ELF signal strengths are very sensitive to sporadic E-layers, with the altitude of the ledge being a very critical parameter.
- o The measured and predicted effects of energetic electron precipitation events can provide a readily available verification of the effects on ELF transmission of more rarely occurring and possibly more severe phenomena such as solar particle events.
- o Variations in the nighttime ELF signal strengths on a fine time scale are observed which may be due entirely to electron precipitation, but cannot be accounted for quantitatively due to present limitations in the measurements and computational techniques.
- o The geometry for the effect of electron precipitation on nighttime ELF transmission is very complex and as a result the following recommendations were made for future investigations:
- o New techniques for mapping electron precipitation profiles simultaneously over a broad spatial region should be used in a coordinated measurement program.
- o Existing ELF waveguide-mode computer programs should be modified to include treatment of variations in the electron and ion density profiles along a direction perpendicular to the propagation path.

In other previous work (Imhof et al., 1978) the findings of an investigation undertaken with coordinated satellite-ELF transmission measurements performed during the Greenland Sea exercise in April - May 1977 were presented. At the same time that the transmission measurements were performed, the Lockheed experiment on the 1972-076B satellite was operated in special coordination to measure the fluxes and energy spectra of the precipitating electrons. This coordinated data set encompassed periods of major geomagnetic disturbance and moderately intense electron precipitation. Calculations of the expected ELF attenuations

were made using the waveguide model computer program developed at the Naval Ocean Systems Center and ionization profiles derived from the satellite measurements of the precipitating electrons. The results have confirmed the previous conclusion that the electron precipitation events occurring along the signal path may lead to either an increase or a decrease in ELF signal attenuation depending on the intensity and location of the ionization.

Further studies were made with data acquired during the electron precipitation event of 26 March 1976. The ELF signal propagation was calculated for a number of paths, from WTF to Maryland, Connecticut, Pisa, Tromso, and Thule. The paths were segmented to take into account the variations of ionization and earth conductivity along the direction of propagation. The results have again emphasized the need for complete information along the path and the difficulty of obtaining it in electron precipitation events with a limited number of satellite passes and without the use of a widespread x-ray mapping technique from a satellite.

Calculations were also performed of the ELF signal transmission from the transmitter at WTF to a receiver at Tromso, Norway during a simulated solar particle event (SPE) under daytime conditions. For these calculations the ion and electron density altitude profiles were based largely on the SPE of 4 August 1972. These daytime results predict a large increase in attenuation over ambient nighttime conditions and a smaller increase over a similar calculation for SPE nighttime conditions.

The purpose of the present report is principally to present further work on the effect of solar particle (PCA) events on ELF propagation. A study was made of observational criteria for selection of a suitable event for a field test of ELF propagation for comparison with propagation code predictions. Improvements were incorporated into a computer code used for calculation of ion and electron densities in PCA conditions, and further study was made of the effects of Sporadic-E layers on ELF propagation during a PCA event.

An intercomparison was made of the calculations of ELF propagation over the WTF to Tromso path performed by three laboratories: LMSC, Naval Ocean Systems Center

(W. Moler), and Pacific Sierra Research (E. C. Field). These calculations were made using five daytime and nighttime test profiles of ion and electron densities provided by LMSC (J. B. Reagan). The results of the comparison show a considerable measure of agreement but illustrate the importance of segmentation of the path and selection of ground conductivities.

A study was made of the expected effect of local time variations during solar particle events on the ELF propagation over the path from WTF to Tronso. Electron and ion density profiles for the various segments of the test path were calculated with the ion chemistry model, taking into account the local time for each segment. In a comparison of conditions measured and calculated for SPE 72 on 4 August 1972 near the peak of the event and conditions calculated for a similar case assuming a season of 21 December, very little difference in signal strength attenuation over the path was found.

A criterion is suggested for determination of a PCA event suitable for an ELF propagation field experiment based on satellite measurements of precipitating proton fluxes. The best times of day for avoidance of twilight over the WTF-Tromso path to minimize ion chemistry modeling problems were described. Also the hours at which ELF noise is least intense were specified. It is shown that sporadic-E effects near the WTF-Tromso path can have a major effect on ELF propagation during a solar particle event.

The ion chemistry model is based on measurements performed during the intense solar particle events of August 1972 and November 1969. The 1972 measurements of electron density were made using the SRI Chatanika incoherent scatter radar. Recent theoretical studies indicate that to obtain correct electron densities the effects of negative ions must be taken into account. Accordingly, the densities for the August 1972 SPE have been revised and the required model revisions have been made with emphasis placed on using the available data at the lower altitudes 60-50 km which are more important for ELF propagation.

Many individuals have contributed significantly to this program. Special acknowledgments are extended to Mr. R. G. Joiner of the Office of Naval Research for

his important cooperation, support, and direction under Contract N00014-79-C-0175. We acknowledge the cooperation of the Norwegian Defense Research Establishment in granting Dr. T. Larsen a leave of absence to engage in this ELF study activity while in residence at LPARL. The assistance and cooperation of Drs. R. Vondrak and J. Vickrey of SRI International in providing additional electron density data for SPE 72 and in clarifying some details of the negative ion correction procedure is gratefully acknowledged.

Section 2

ELF CODE INTERCOMPARISON USING PCA IONOSPHERIC PROFILES SUPPLIED BY LMSC

In 1978 as part of the DNA DISMEDIA program effort, LMSC (J. B. Reagan, private communication) provided to the ELF propagation community a set of electron and ion density altitude profiles for PCA conditions. This set included profiles for three daytime and two nighttime cases. These profiles are specified in Figures 2.1 and 2.2 and in Tables 2.1, 2.2, and 2.3.

The PCA Day #1 profile represented the conditions near the peak of SPE72 at 1508 UT on 4 August when the solar zenith angle χ was 79.5^{o}. The ion pair production rate at 40 km was the largest measured to date in a solar particle (PCA) event for altitudes between 50 and 100 km. The electron density (N_e) values were derived from Chatanika radar measurements. At altitudes below 50 km calculations were performed using an ion-neutral chemistry code developed by Gunton et al. (1977). The positive ion densities were obtained with use of the same code at heights between 80 and 40 km, and from the relationship $N_+ = (q/\alpha_i)^{1/2}$ at lower altitudes where the ion neutralization rate α_i was given the altitude variation described in Imhof et al (1978). The ion pair production rates q were derived from satellite measurements made by LMSC (Reagan and Watt, 1976).

It should be noted here that recent theoretical developments show that the influence of negative ions must be taken into account when deriving N_e values from the Chatanika radar measurements. The corrected electron densities are lower than previously thought, up to a factor of two, and positive ion densities are larger above ~40 km. These corrections are described in detail in Section 7 of this report. The profiles discussed in this section are, however, uncorrected and the electron densities are larger than they should be.

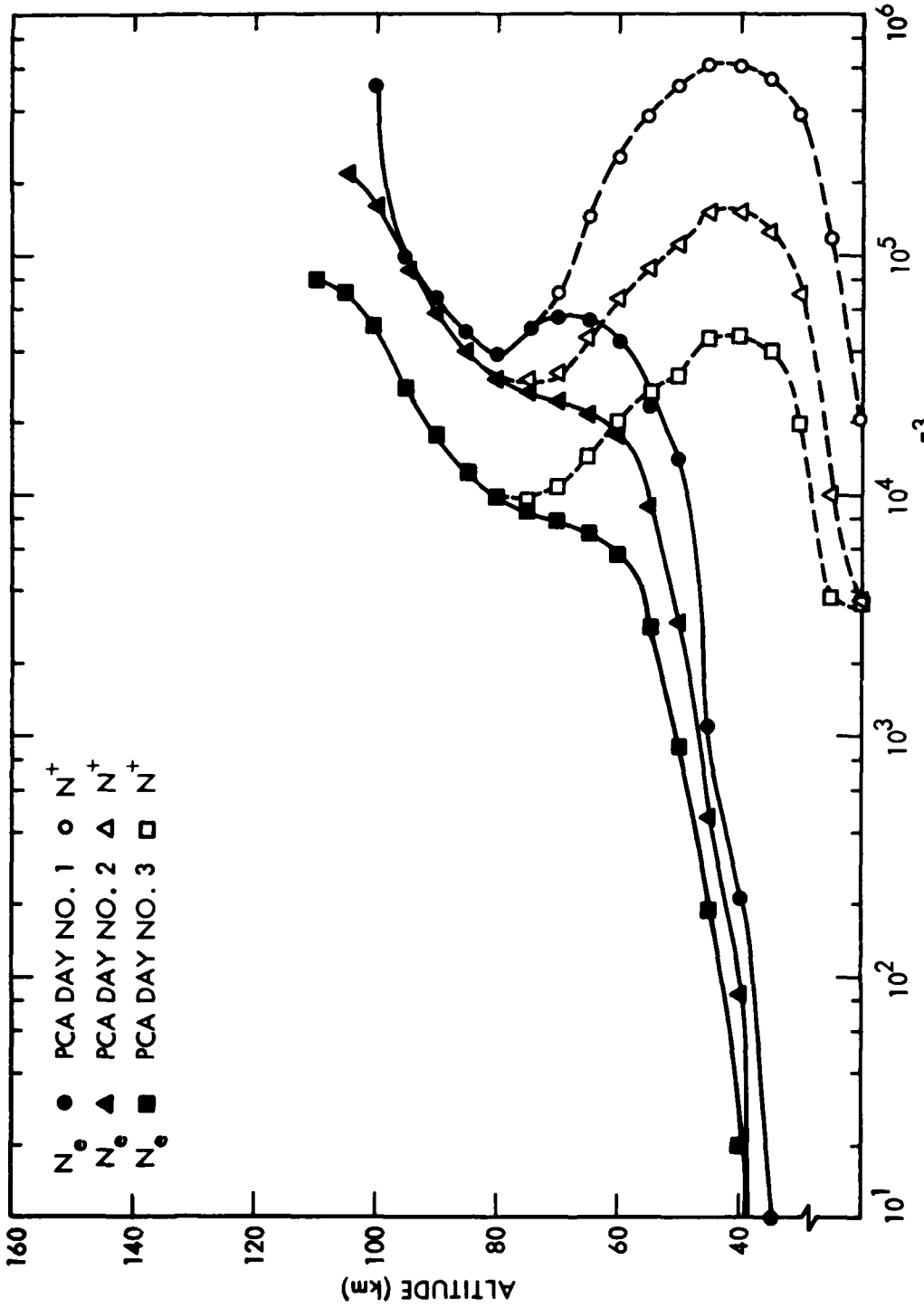

Figure 2.1 Electron and ion density profiles for the PCA daytime test cases

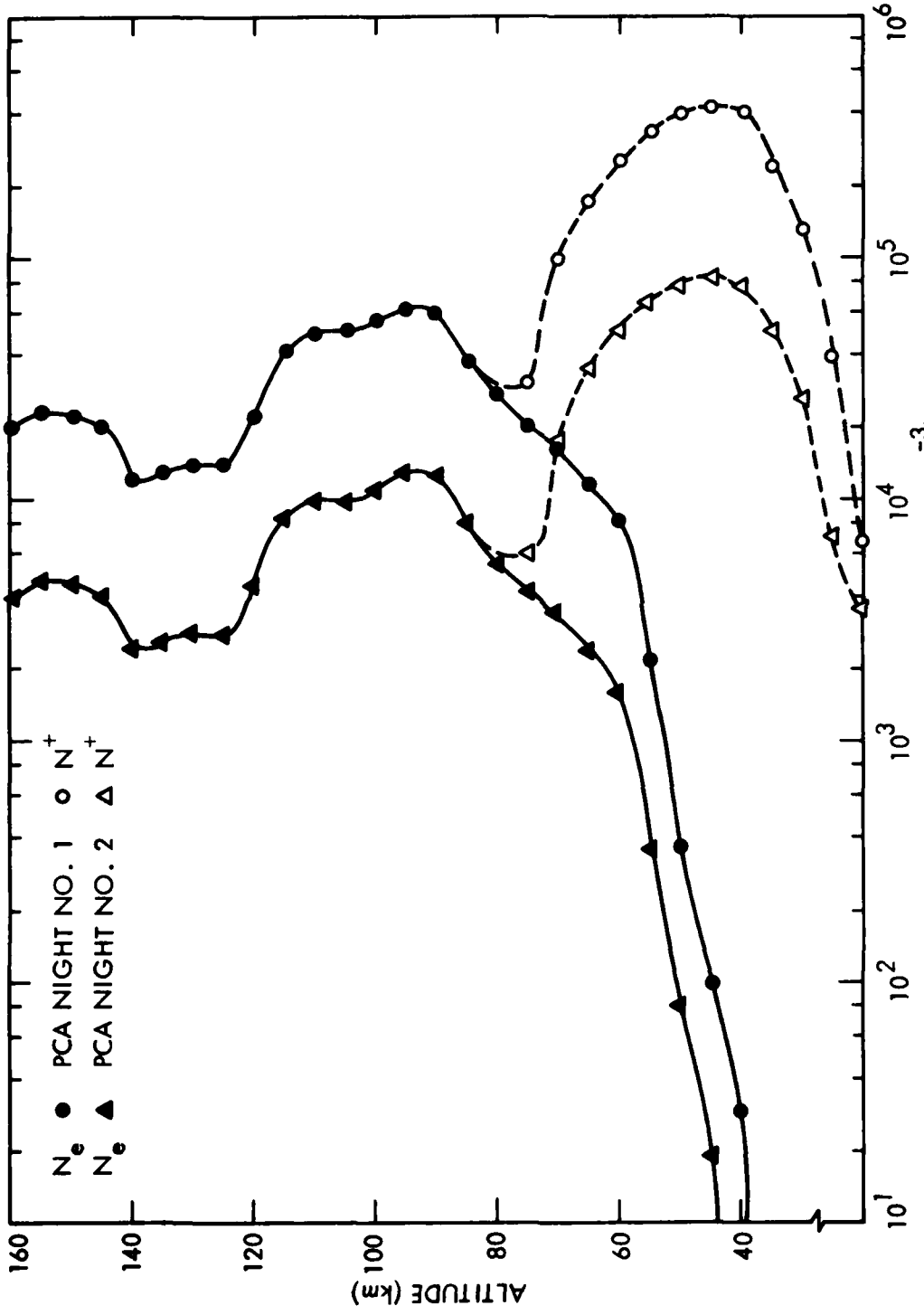

Figure 2.2 Electron and ion density profiles for the PCA nighttime test cases

Table 2.1 Electron density vs height for PCA daytime test cases.

Altitude (km)	PCA Day #1 (cm-3)	PCA Day #2 (cm-3)	PCA Day #3 (cm-3)
110			7.80 (4)
105		2.20 (5)	7.00 (4)
100	5.00 (5)	1.60 (5)	5.00 (4)
95	1.00 (5)	8.80 (4)	2.80 (4)
90	6.50 (4)	5.70 (4)	1.80 (4)
85	4.80 (4)	4.00 (4)	1.25 (4)
80	3.80 (4)	3.10 (4)	1.00 (4)
75	5.00 (4)	2.75 (4)	8.80 (3)
70	5.50 (4)	2.50 (4)	7.90 (3)
65	5.40 (4)	2.20 (4)	7.00 (3)
60	4.50 (4)	1.80 (4)	5.60 (3)
55	2.30 (4)	9.00 (3)	2.90 (3)
50	1.40 (4)	2.90 (3)	9.00 (2)
45	1.10 (3)	4.65 (2)	1.90 (2)
40	2.15 (2)	8.65 (1)	2.00 (1)
35	1.00 (1)	3.47 (-4)	3.47 (-4)
30	1.67 (-4)	1.67 (-4)	1.67 (-4)
25	7.70 (-5)	7.70 (-4)	7.70 (-5)
20	3.43 (-5)	3.43 (-5)	3.43 (-5)
15	1.50 (-5)	1.50 (-5)	1.50 (-5)
10	6.58 (-6)	6.58 (-6)	6.58 (-6)
5	3.43 (-6)	3.43 (-6)	3.43 (-6)
0	0	0	0

Table 2.2 Positive ion densities vs height in PCA daytime test cases.

Altitude (km)	PCA Day #1 (cm-3)	PCA Day #2 (cm-3)	PCA Day #3 (cm-3)
110			7.80 (4)
105		2.20 (5)	7.00 (4)
100	5.00 (5)	1.60 (5)	5.00 (4)
95	1.00 (5)	8.80 (4)	2.80 (4)
90	6.50 (4)	5.70 (4)	1.80 (4)
85	4.80 (4)	4.00 (4)	1.25 (4)
80	3.80 (4)	3.10 (4)	1.00 (4)
75	5.00 (4)	2.95 (4)	9.70 (3)
70	7.00 (4)	3.20 (4)	1.10 (4)
65	1.40 (5)	4.50 (4)	1.45 (4)
60	2.50 (5)	6.50 (4)	2.00 (4)
55	3.70 (5)	8.60 (4)	2.70 (4)
50	5.00 (5)	1.10 (5)	3.10 (4)
45	6.00 (5)	1.50 (5)	4.50 (4)
40	6.00 (5)	1.50 (5)	4.55 (4)
35	5.40 (5)	1.25 (5)	4.00 (4)
30	3.75 (5)	6.90 (4)	2.00 (4)
25	1.15 (5)	1.00 (4)	3.70 (3)
20	2.05 (4)	3.65 (3)	3.50 (3)
15	3.63 (3)	3.63 (3)	3.70 (3)
10	3.72 (3)	3.72 (3)	3.72 (3)
5	4.48 (3)	4.48 (3)	4.48 (3)
0	0	0	0

Table 2.3 Electron and positive ion density vs height for PCA nighttime test cases.

Altitude (km)	Ne (cm^{-3})		N^+ (cm^{-3})	
	PCA night #1	#2	PCA night #1	#2
250	1.00 (5)	1.00 (5)		
225	1.45 (4)	5.00 (3)		
220	1.30 (4)	3.20 (3)		
210	1.30 (4)	2.60 (3)		
200	1.45 (4)	2.80 (3)		
190	1.70 (4)	3.40 (3)		
180	2.00 (4)	4.00 (3)		
170	2.25 (4)	4.50 (3)		
160	2.35 (4)	4.80 (3)		
155	2.30 (4)	4.60 (3)		
150	2.20 (4)	4.40 (3)		
145	2.00 (4)	4.00 (3)	N^+=Ne	N^+=Ne
140	1.20 (4)	2.40 (3)	#1	#2
135	1.30 (4)	2.60 (3)		
130	1.40 (4)	2.80 (3)		
125	1.40 (4)	2.80 (3)		
120	2.20 (4)	4.40 (3)		
115	4.20 (4)	8.40 (3)		
110	4.90 (4)	9.90 (3)		
105	5.00 (4)	1.00 (4)		
100	5.60 (4)	1.10 (4)		
95	6.40 (4)	1.28 (4)		
90	6.20 (4)	1.25 (4)		
85	3.80 (4)	8.00 (3)		
80	2.80 (4)	5.40 (3)	3.00 (4)	5.80 (3)
75	2.00 (4)	4.10 (3)	3.00 (4)	6.00 (3)
70	1.70 (4)	3.40 (3)	1.00 (5)	1.80 (4)
65	1.20 (4)	2.40 (3)	1.70 (5)	3.50 (4)
60	8.60 (3)	1.60 (3)	2.50 (5)	5.00 (4)
55	2.20 (3)	3.60 (2)	3.30 (5)	6.50 (4)
50	3.80 (2)	8.20 (1)	3.90 (5)	7.70 (4)
45	1.00 (2)	1.90 (1)	4.10 (5)	8.30 (4)
40	3.00 (1)	5.80 (0)	4.00 (5)	7.80 (4)
35	3.50 (-4)	9.00 (-3)	2.40 (5)	5.00 (4)
30	1.70 (-4)	3.30 (-4)	1.30 (5)	2.60 (4)
25	7.70 (-5)	7.70 (-5)	3.90 (4)	7.00 (3)
20	3.43 (-5)	3.43 (-5)	6.70 (3)	3.50 (3)
15	1.50 (-5)	1.50 (-5)	3.63 (3)	3.80 (3)
10	6.58 (-6)	6.58 (-6)	3.72 (3)	3.72 (3)
5	3.43 (-6)	3.43 (-6)	4.48 (3)	4.48 (3)
0	0	0	0	0

The PCA Day #2 profiles represent later less disturbed conditions in SPE 72 on 5 August at 0306 UT when χ was 69.3^{o}.

The PCA Day #3 profile is scaled down from #2, with all densities reduced by a factor of about $\sqrt{10}$ corresponding approximately to q values scaled down by an order of magnitude. Case #3 may be close to the minimum desired SPE for test purposes.

The Night Case #1 profiles were based on SPE 72 on 4 August at 1144 UT when χ was 95.3^{o}. This was actually a deep twilight case since sunset was not complete at the higher altitudes above about 50 km.

Night Case #2 was scaled down from #1 by a factor of about 5 in the electron and ion densities to represent a minimum desired SPE for testing, although it still represents a severe night disturbance.

These profiles have been used by W. Moler of the Naval Ocean Systems Center (NOSC), by E. C. Field of Pacific Sierra Research (PSR), as well as by LMSC as input for ELF propagation computations for selected paths starting from the Wisconsin Test Facility (WTF). The LMSC calculations were made with the NOSC Code (Pappert and Moler, 1974) kindly furnished by W. Moler. All of the results cited here are for the WTF to Tromso test path. The path is segmented to provide for variation of ground conductivity and magnetic field. The segmentation of the path in the LMSC calculations is the same as that used previously and is shown in Table 2.4 which also shows the propagation characteristics for various segments in the daytime cases. Table 2.5 shows similar results for the nighttime cases.

In calculation of a given case, the electron and ion density profiles are the same in all segments of the path.

The resulting attenuations specified relative to ambient conditions as calculated at the three laboratories are given in Table 2.6. For these same cases the absolute field strengths computed by LMSC and NOSC at the receiver are given in

Table 2•4. Propagation characteristics, attenuation, relative phase velocity, and excitation factor at 75 Hz for the WTF to Tromso path for ambient daytime and PCA daytime and PCA daytime test cases.

		Day Ambient			PCA Day #1			PCA Day #2			PCA Day #3		
	Segment	Attn.	v/c	Exc. Fac.	Attn.	v/c	Exc. Fac.	Attn.	v/c	Exc. Fac.	Attn.	v/c	Exc. Fac.
1	WTF Area	1.37	0.82	-3.22	2.61	0.74	3.15	2.03	0.77	1.24	1.94	0.77	0.50
2	Canada	1.31	0.83	-3.27	2.50	0.74	3.06	1.93	0.78	1.15	1.85	0.78	0.43
3	Hudson Bay	1.22	0.83	-3.34	2.35	0.75	2.96	1.80	0.78	1.05	1.73	0.79	0.33
4	N. Canada	1.30	0.83	-3.28	2.50	0.74	3.06	1.93	0.78	1.15	1.84	0.78	0.43
5	Davis Strait	1.22	0.83	-3.36	2.35	0.75	2.96	1.80	0.78	1.05	1.72	0.79	0.33
6	Greenland	2.03	0.79	-2.63	3.72	0.70	4.00	3.00	0.73	2.05	2.82	0.74	1.28
7	Norwegian Sea	1.19	0.83	-3.39	2.35	0.75	2.96	1.80	0.78	1.05	1.709	0.79	0.33
8	Tromso Area	1.27	0.83	-3.32	2.50	0.74	3.06	1.92	0.78	1.15	1.82	0.78	0.43

Note: In the field strength calculations for WTF to Tromso for the PCA daytime cases the standard daytime ambient has been used for Segment #1.

Table 2·5. Propagation characteristics attenuation, relative phase velocity, and excitation factor at 75 Hz for propagation from WTF to Tromso for ambient and PCA nighttime conditons.

Segment		Ambient Night			PCA Night #1			PCA Night #2		
		Attn. dB/Mm	v/c	Exc. Fac.	Attn.	v/c	Exc. Fac.	Attn.	v/c	Exc. Fac.
1	WTF Area	1.09	0.85	-5.46	2.52	0.74	2.30	2.63	0.75	0.63
2	Canada	1.04	0.85	-5.52	2.41	0.74	2.23	2.49	0.76	0.54
3	Hudson Bay	0.97	0.86	-5.59	2.28	0.75	2.13	2.38	0.76	0.45
4	N. Canada	1.03	0.85	-5.51	2.41	0.74	2.22	2.52	0.76	0.56
5	Davis Strait	0.95	0.86	-5.58	2.28	0.75	2.12	2.46	0.76	0.48
6	Greenland	1.64	0.82	-4.91	3.51	0.70	3.07	3.58	0.72	1.33
7	Norwegian Sea	0.90	0.86	-5.55	2.26	0.75	2.12	2.64	0.77	0.39
8	Tromso Area	0.96	0.85	-5.49	2.39	0.74	2.22	2.75	0.77	0.46

Note: In the field strength calculations for PCA Night #1 and #2 the nighttime ambient profile has been used for the first segment.

Table 2.6 Computed change in ELF field strength in going from ambient day and ambient night conditions to PCA conditions. The calculations refer to transmission from WTF to Tromso at 75 Hz.

	LMSC	NOSC	PSR
PCA Day #1	-5.7 dB	-3.8 dB	-5.6 dB
#2	-2.8	-1.0	-3.9
#3	-2.3	-1.3	-3.7
PCA Night #1	-6.4	-6.8	--
#2	-7.9	-6.2	--

Table 2.7. The NOSC field strengths have all been adjusted to account for a different assumption about ground conductivity under the WTF transmitter antenna.

The relative field strengths in Table 2.6 show some differences between laboratories. The absolute values in Table 2.7 generally indicate agreement to about 1 dB for each case.

INFLUENCE OF THE SIZE OF THE FIRST SEGMENT UPON THE ELF FIELD STRENGTHS

The WTF transmitter region has low ground conductivity @ 75 H_z $\sigma \sim 3.2 \times 10^{-4}$ mho/m . The extent of this region is taken to be 200 km in our segmentation of the ELF paths. W. Moler, NOSC, used 500 km for the transmitter region. However at 500 km from WTF part of Lake Superior, $\sigma \sim$ 4 mho/m, is included. Thus the analyst faces a dilemma in choosing the size of the first segment.

One run was made for PCA night #2 for which we extended the first segment out to 900 km. The results were:

PCA night #2 (Segment 1 size 200 km) - 162.6 dB
PCA night #2 (Segment 1 size 900 km) - 161.5 dB

It is thus obvious that the size of the segments for the WTF area is of importance, especially when one tries to compare results from various codes, in absolute terms.

COMMENTS ON THE COMPARISON BETWEEN LMSC AND NOSC FIELD STRENGTH CALCULATIONS

As pointed out above most of the computed values in Table 2.7 agree within approximately 1 dB in absolute field strength. This raises the question as to why perfect agreement is not attained since the same code is used. The following factors are involved:

- o In running the code with elaborate segmentation of the path it is difficult to avoid introducing differences, e.g.,

Table 2•7. Comparison between ELF absolute field strength calculations at 75Hz for the path WTF to Tromso*.

Condition	LMSC dB/1A/m	NOSC dB/1A/m
Day, ambient	-154.7	-155.4
Night, ambient	-154.7	-154.6
Day PCA #1	-160.4	-159.2
Day PCA #2	-157.5	-156.4
Day PCA #3	-157.0	-156.7
Night PCA #1	-161.1	-161.4
Night PCA #2	-162.6	-160.8

*The field strength values in this table and in all other references in this report have been normalized to include the signal of the WTF E-W antenna in addition to that of the N-S antenna which is computed by the waveguide mode code: The E-W antenna conditions are: Current 300A; length 22.5 km, conductivity of ground under antenna 3.2×10^{-4} mho/m; phasing between E-W and N-S antennas - 0°.

The NOSC data supplied by W. Moler have been adjusted by -1.6dB due to a different value used for the soil conductivity under the WTF transmitter (NOSC data were actually computed for $\sigma = 2.2\ 10^{-4}$ mho/m, whereas the field strength values in the table are normalized to $\sigma = 3.2\ 10^{-4}$ mho/m, which is used by LMSC).

- o The actual number of segments used may differ
- o The positions and lengths of the individual segments may vary
- o Values of the ground conductivities may be chosen differently
- o The size of the WTF area may not be exactly the same
- o The N_e, N_+ profiles supplied by LMSC needed some extrapolation to F region altitudes (PCA night #2) and to very low altitudes. These extrapolations may introduce minor differences.

It appears probable that a major item involves the different sizes of the WTF region used by LMSC and NOSC, which are 200 km and 500 km, respectively.

ELF PROPAGATION CHARACTERISTICS - SENSITIVITY TO N_e AND N_+ ALTITUDE PROFILES

A comparison between altitude profiles of the Joule heating calculated by E. C. Field and by W. Moler for PCA day test case #1 is given in Figure 2.3. The curves have been normalized to provide equal values at the lower maximum in the 30-35 km altitude regime and they indicate that a reasonable agreement exists between two approaches. Both calculations show that the largest attenuation of 75 Hz waves occurs between approximately 25 and 40 km with a secondary maximum around 60 km. The former maximum may be linked with high ion densities, whereas the latter maximum is mainly due to the free electrons.

Using the PCA day- and nighttime test cases supplied by LMSC, W. Moler at NOSC has calculated in addition to the Joule heating the altitude variation for the integrated absorptions and the reflection density of the downgoing wave for these conditions. When compared with the actual electron and ion density variation with height, the variations of the above entities reveal interesting characteristics of ELF propagation.

As an example, in Figures 2.4 and 2.5 we have plotted the profiles for the PCA day test case #1 for 75 Hz). Figure 2.4 clearly shows the importance of the enhanced ion concentration, peaking approximately at 40 km. The relative heating loss (dotted curve) indicates that the maximum Joule heating occurs at 35 km. Integrated absorption in dB/1000 km (dash-dotted curve) furthermore

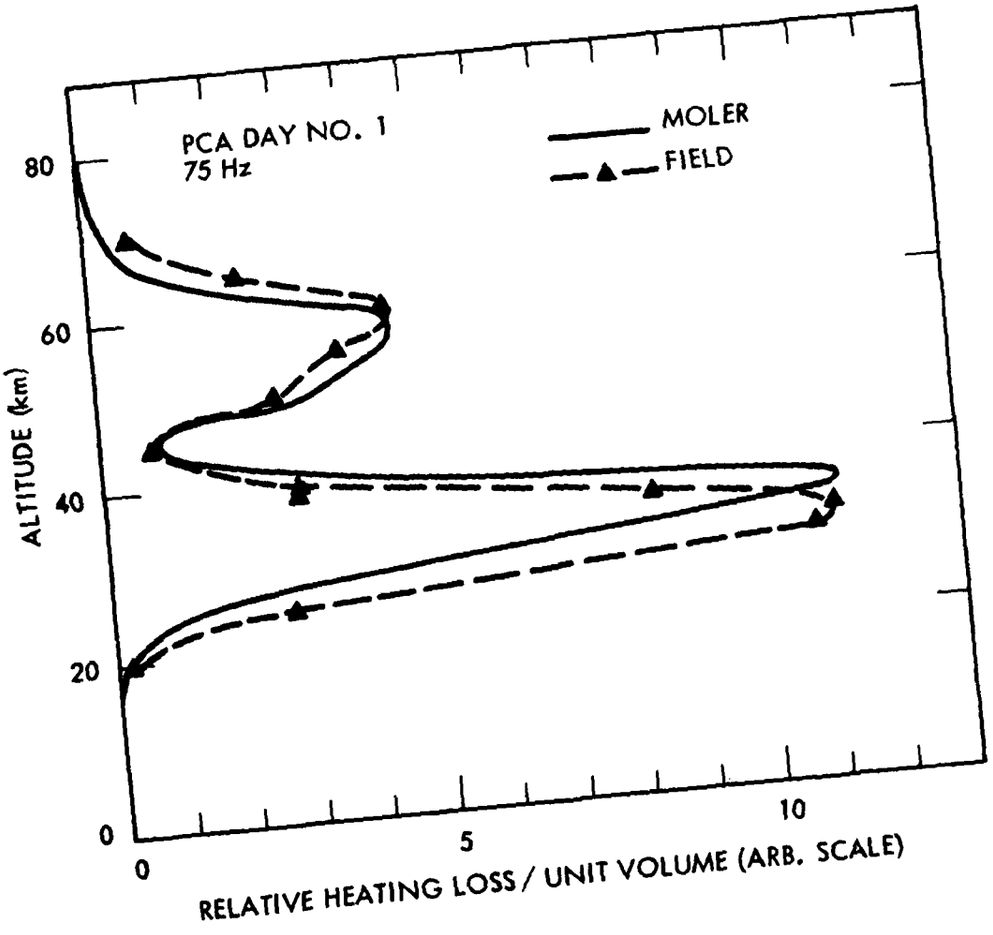

Figure 2.3. Comparison of Joule heating for PCA day test case #1 by E. C. Field (PSR) and W. Moler (NOSC). The curves have been normalized to give equal values at the lower maximum.

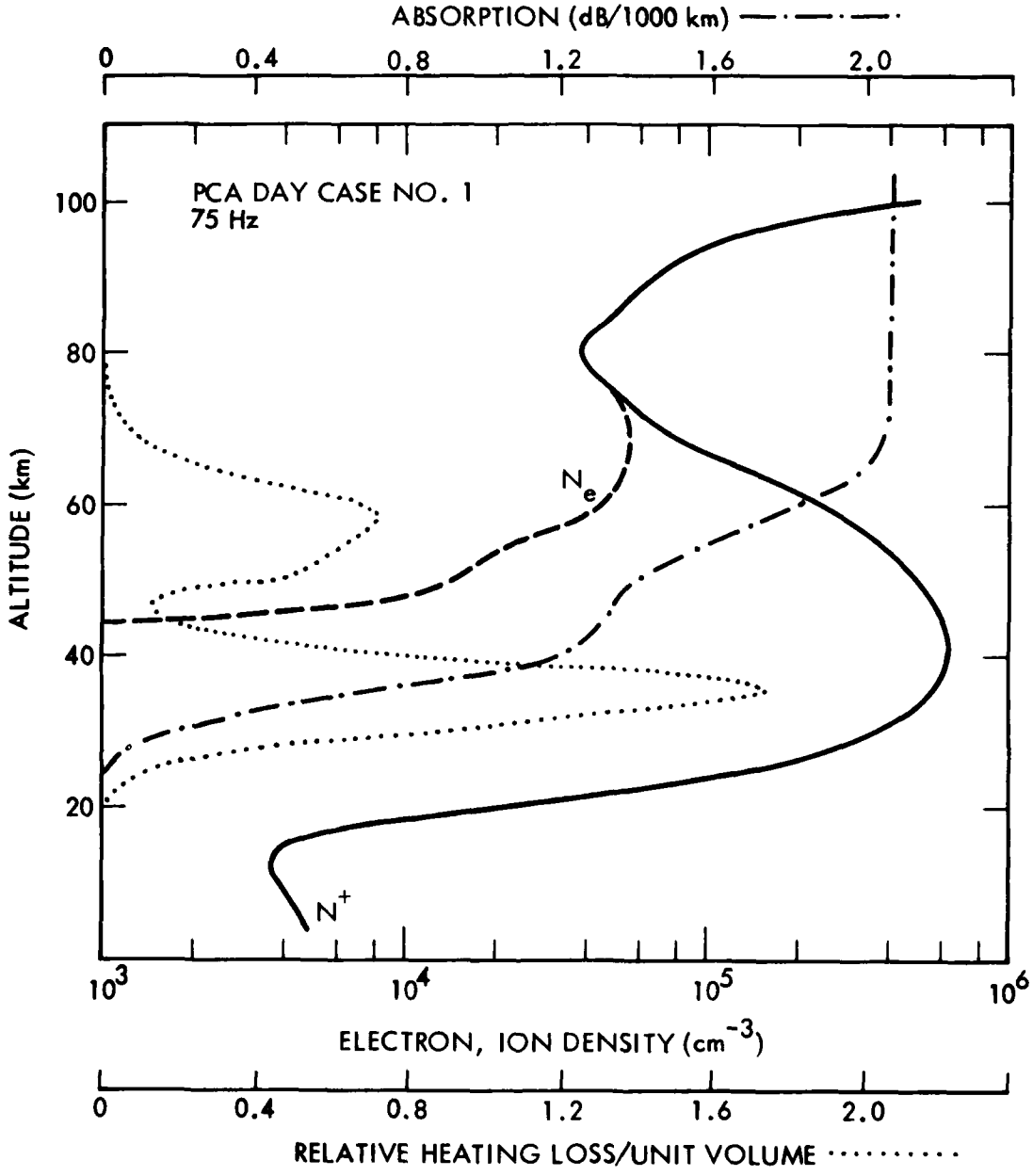

Figure 2•4.

Altitude variation of ionospheric and ELF characteristics for PCA daytime conditions (test case #1).

- o N_+, ion density (heavy, solid curve)
- o N_e, electron density (heavy, dashed curve)
- o Relative heating loss/unit volume (dotted curve)
- o Integrated Absorption (dB/1000 km) (dash-dotted curve)

The last two curves were computed by W. Moler, NOSC for a frequency of 75Hz for the pictured N_+ and N_e profiles (Moler, 1978) .

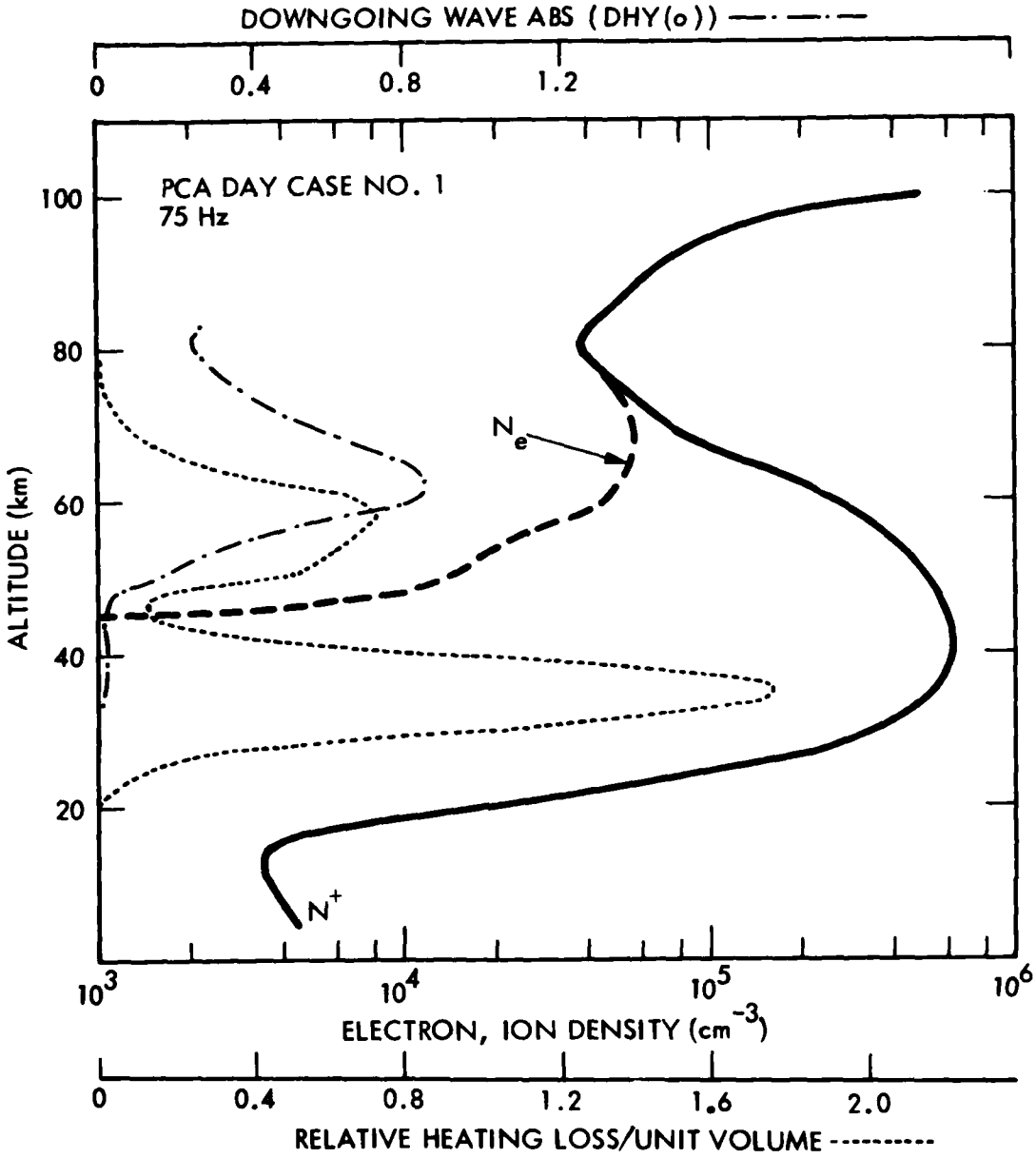

Figure 2•5.

Altitude variation of ionospheric and ELF characteristics for PCA daytime conditions (test case #1)

- o N_+, ion density (heavy, solid curve)
- o N_e, electron density (heavy, dashed curve)
- o Relative heating loss/unit volume (dotted curve)
- o Reflection density of downgoing wave (H_y)

The last two curves were computed by W. Moler, NOSC for a frequency of 75Hz for the pictured N_+ and N_e profiles (Moler, 1978). For further explanation of the last two curves see Pappert and Shockey (1977).

shows that approximately 1.3 dB out of the total 2.1 dB/1000 km can be associated with this layer. The free electrons cause Joule heating mainly at higher altitudes, maximizing around 60 km. In Figure 2.4 the reflection density profile of the downgoing wave (dash-dotted curve) indicates that the region between 50 and 80 km is the main reflecting region during the PCA conditions.

Figures 2.6 and 2.7 show the same entities as Figure 2.4 and 2.5, respectively, but for quiet, ambient nighttime conditions. In this case the ELF fields penetrate to greater heights before reflection takes place. Figure 2.6 shows that the Joule heating, essentially due to electrons, occurs within quite a narrow altitude interval between 65 and 75 km, whereas the ions cause another maximum at around 110 km. Also, in this case there is only an insignificant contribution to the attenuation from Joule heating below 40 km. Figure 2.7 indicates that significant contributions to the $H\phi$ field (at ground level) are coming from altitudes between 100-120 km (dash-dotted curve), but that altitudes up to about 160 km do contribute.

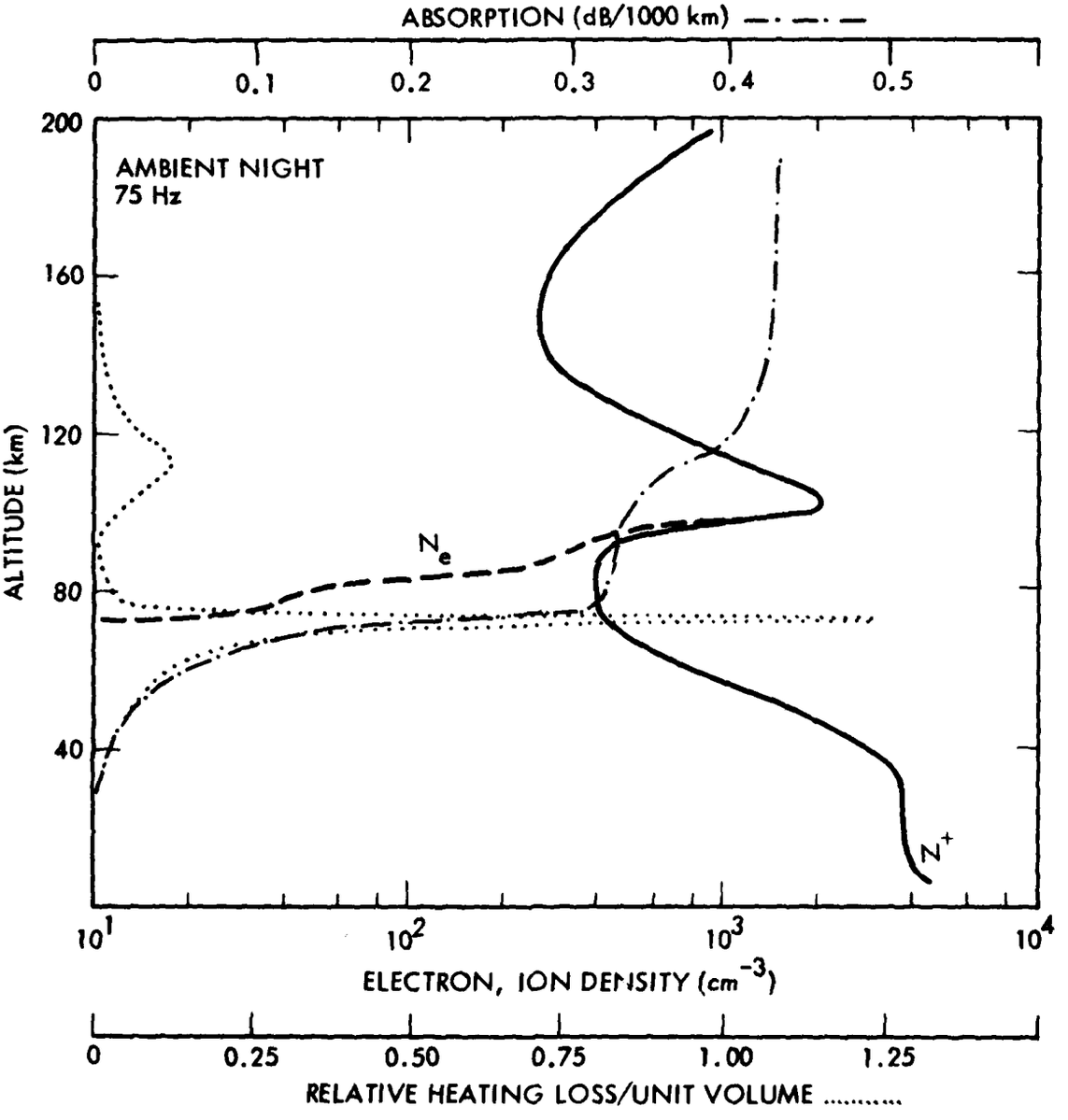

Figure 2.6. Altitude variation of ionospheric and ELF characteristics for ambient nighttime conditions. For explanation, refer to Figure 2.4.

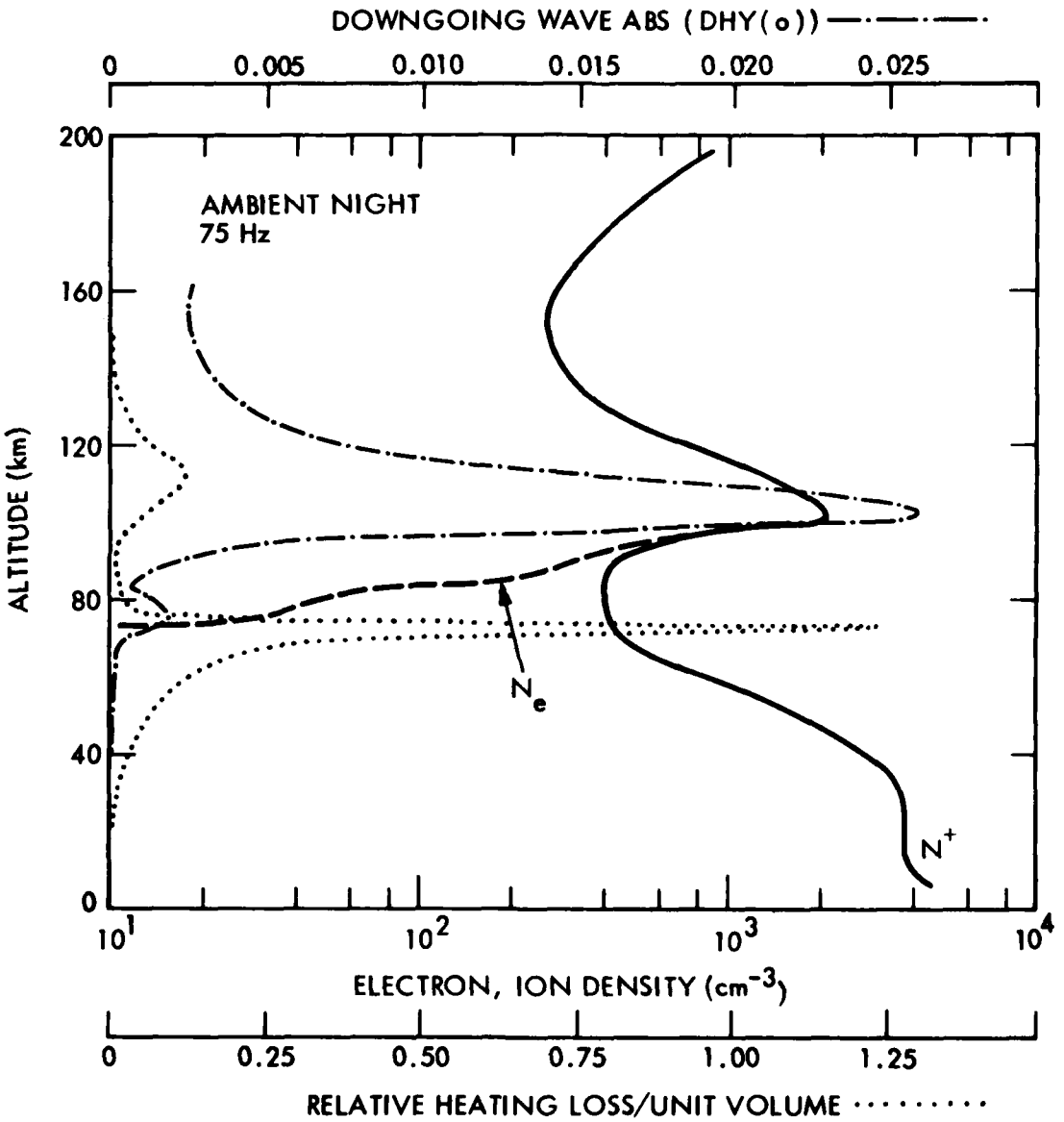

Figure 2.7. Altitude variation of ionospheric and ELF characteristics for ambient nighttime conditions. For explanation, refer to Figure 2.5.

Section 3
STANDARD AMBIENT DAY AND NIGHT CONDITIONS

In this report we compare many of our calculations over the ELF propagation path WTF to Tromso with the standard day and night conditions which have been used in this program. The electron and ion density proviles used as standards are shown in Figure 3.1. These profiles are presented for convenience in Tables 3.1 and 3.2. When the total attenuation over the WTF to Tromso path is computed for ambient daytime conditions in all segments of the path the result is -154.7 dB. When the nighttime profile is used in all segments the result is fortuitously the same number. This result may be understood by reference to Table 3.3 which shows the attenuations and excitation factors. For the ambient daytime conditions the attenuations and the excitation factors are greater than for ambient night. Plots of total attenuation vs. distance along the path shown in Figure 3.2 illustrate the fortuitous crossing at 6 Mm, the WTF-Tromso distance. The results for the case PCA Night #1 in the same figure show the effect of the greater attenuations under excited conditions.

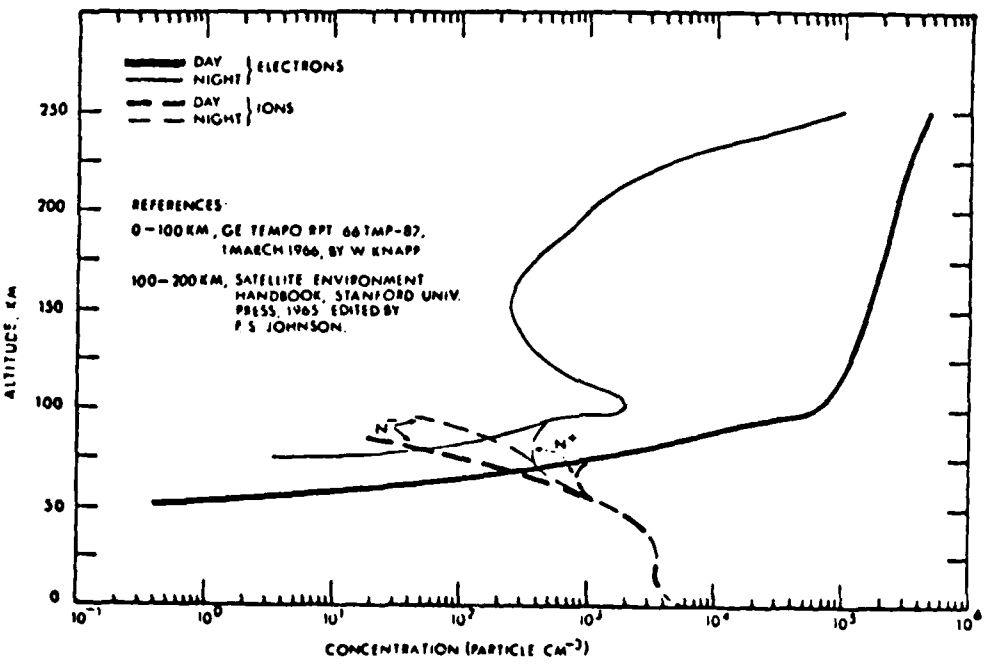

Figure 3.1. Standard Ambient Electron and Ion Density Profiles.

Table 3.1. Ambient daytime electron and positive ion densities (cm^{-3}).

Altitude (km)	Ambient Day	
	Ne	N^+
160	1.80 (5)	1.80 (5)
150	1.60 (5)	1.60 (5)
140	1.50 (5)	1.50 (5)
130	1.30 (5)	1.30 (5)
120	1.10 (5)	1.10 (5)
110	8.60 (4)	8.60 (4)
100	6.00 (4)	6.00 (4)
95	3.60 (4)	3.60 (4)
90	1.50 (4)	1.50 (4)
85	7.00 (3)	7.00 (3)
80	3.00 (3)	3.00 (3)
75	1.00 (3)	1.00 (3)
70	2.40 (2)	5.80 (2)
65	4.70 (1)	5.33 (2)
60	6.50 (0)	7.66 (2)
55	7.50 (-1)	1.09 (3)
50	1.00 (-1)	1.54 (3)
45	1.50 (-2)	2.11 (3)
40	3.10 (-3)	2.73 (3)
35	9.20 (-4)	3.25 (3)
30	3.00 (-4)	3.55 (3)
25	1.00 (-4)	3.69 (3)
20	3.43 (-5)	3.65 (3)
15	1.50 (-5)	3.63 (3)
10	6.58 (-6)	3.72 (3)
5	3.43 (-6)	4.48 (3)
0	0	0

Table 3.2. Ambient nighttime electron and positive ion densities (cm^{-3})

Altitude (km)	N_e	N_+	Altitude (km)	N_e	N_+
250	1.00 (5)		95	5.82 (2)	6.30 (2)
225	5.00 (3)		90	3.15 (2)	4.11 (2)
220	3.20 (3)		85	1.97 (2)	4.11 (2)
210	1.68 (3)		80	5.09 (1)	4.11 (2)
200	1.00 (3)		75	3.14 (1)	4.11 (2)
190	6.50 (2)		70	3.27 (-2)	4.11 (2)
180	4.60 (2)		65	1.00 (-2)	5.33 (2)
170	3.45 (2)		60	5.73 (-3)	7.66 (2)
160	2.82 (2)		55	3.39 (-3)	1.09 (3)
155	2.60 (2)		50	2.06 (-3)	1.54 (3)
150	2.50 (2)	$N_e=N_+$	45	1.22 (-3)	2.11 (3)
145	2.55 (2)		40	6.74 (-4)	2.73 (3)
140	2.80 (2)		35	3.47 (-4)	3.25 (3)
130	3.70 (2)		30	1.67 (-4)	3.55 (3)
120	5.80 (2)		25	7.70 (-4)	3.69 (3)
112	1.10 (3)		20	3.43 (-5)	3.65 (3)
106	1.70 (3)		15	1.50 (-5)	3.63 (3)
104	1.90 (3)		10	6.58 (-6)	3.72 (3)
102	1.98 (3)		5	3.43 (-6)	4.48 (3)
100	2.00 (3)		0	0	0
99	1.95 (3)				

Table 3-3. Waveguide characteristics, attenuation and excitation factor, at 75 Hz for ambient day - and nighttime ionospheric profiles over the various path segments for WTF to Tromso.

		Ambient Night		Ambient Day	
	Segment	Att. dB/Mm	Excit. Fac. dB	Att. dB/Mm	Excit. Fac. dB
1	WTF Area	1.09	-5.46	1.37	-3.22
2	Canada	1.04	-5.52	1.31	-3.27
3	Hudson Bay	0.97	-5.59	1.22	-3.34
4	North Canada	1.03	-5.51	1.30	-3.28
5	Davis Strait	0.95	-5.58	1.21	-3.36
6	Greenl. Ice Cap	1.64	-4.91	2.03	-2.63
7	Norwegian Sea	0.90	-5.55	1.19	-3.39
8	Tromso Area	0.96	-5.49	1.27	-3.33

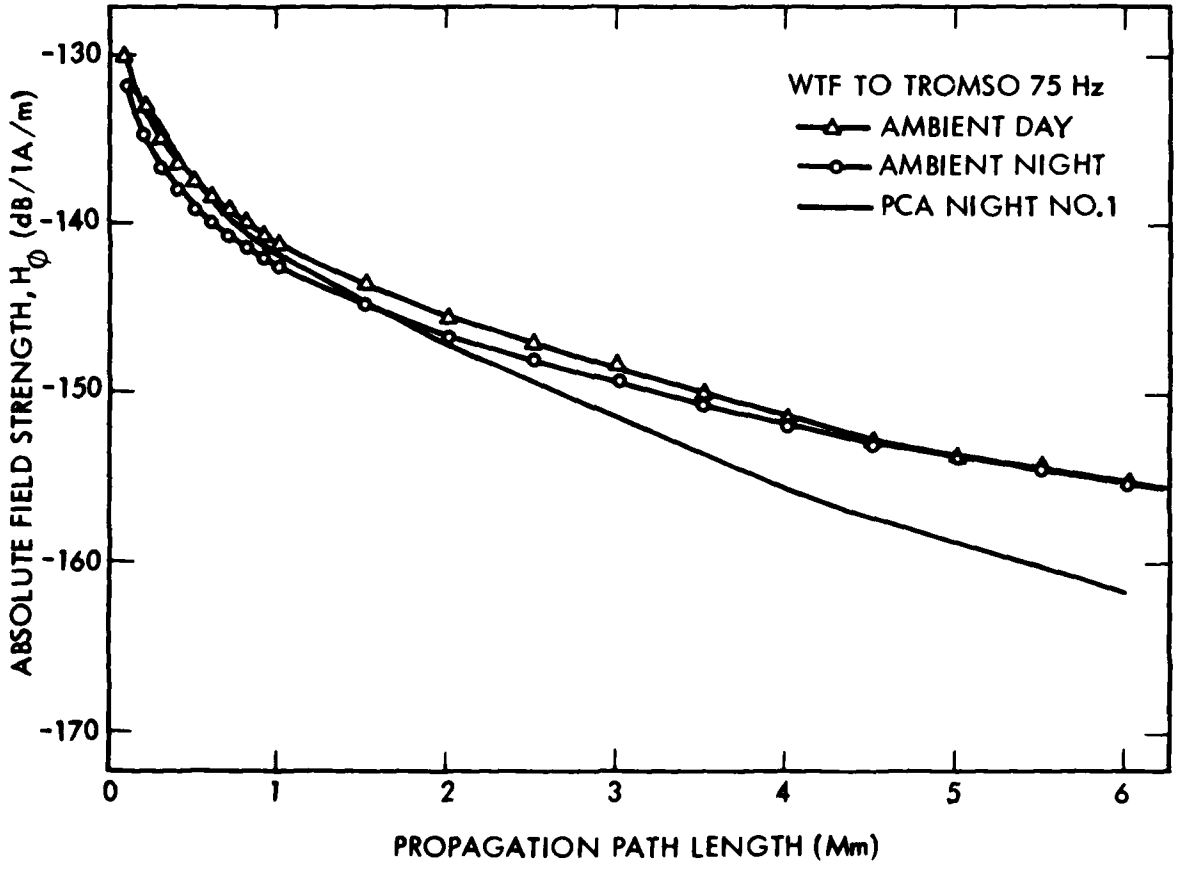

Figure 3.2. Absolute field strength calculated for standard ambient day and ambient night profiles over the path WTF to Tromso showing the fortuitous agreement at 6 megameters. The corresponding result for the PCA nighttime case #1 is also shown.

Section 4

EFFECT OF LOCAL TIME VARIATIONS ON ELF PROPAGATION IN SOLAR PARTICLE EVENTS

Calculations have been made of ELF propagation along the test path from the Wisconsin Test Facility (WTF) to Tromso, Norway shown in Figure 4.1. The purposes of these calculations are to find the possible effects of: (1) the variation of local time along the path, and (2) the influence of gradients perpendicular to the path on possible future three-dimensional (3D) calculations. The revised ion chemistry model has been used to calculate ion and electron densities at the indicated mid points of the eight standard segments in Figure 4.1 at altitudes between 40 and 80 km. The segmentation of the path in the ELF propagation calculations for variations of magnetic field, ground conductivity, and now of charged particle densities follows that of our previous work (Imhof et al, 1977, 1978). At each point in the direct path the atmospheric densities and photo coefficients used in the model were appropriate to the latitude and chosen time of year, December 21. The ion pair production rates used in this simulated solar particle event were those measured in SPE72 with the peak of the ionization occurring near local noon at 45°W longitude. Calculations were made for the direct path, i.e., the great circle path WTF to Tromso, and for two parallel paths separated by about 1100 km to the north and to the south. The points in the two additional paths were treated like the points in the direct path having the same segmentation, atmospheric densities, magnetic field and ground conductivities. Only the photocoefficients and local times were varied to correspond to the new geographical positions in calculating electron and ion densities. The time of this simulated event was set at winter solstice and with local noon at 45°W in an attempt to maximize the differences among the three paths produced by local time and photo effects. The latitudes and local times of the segments of the paths are given in Table 4.1.

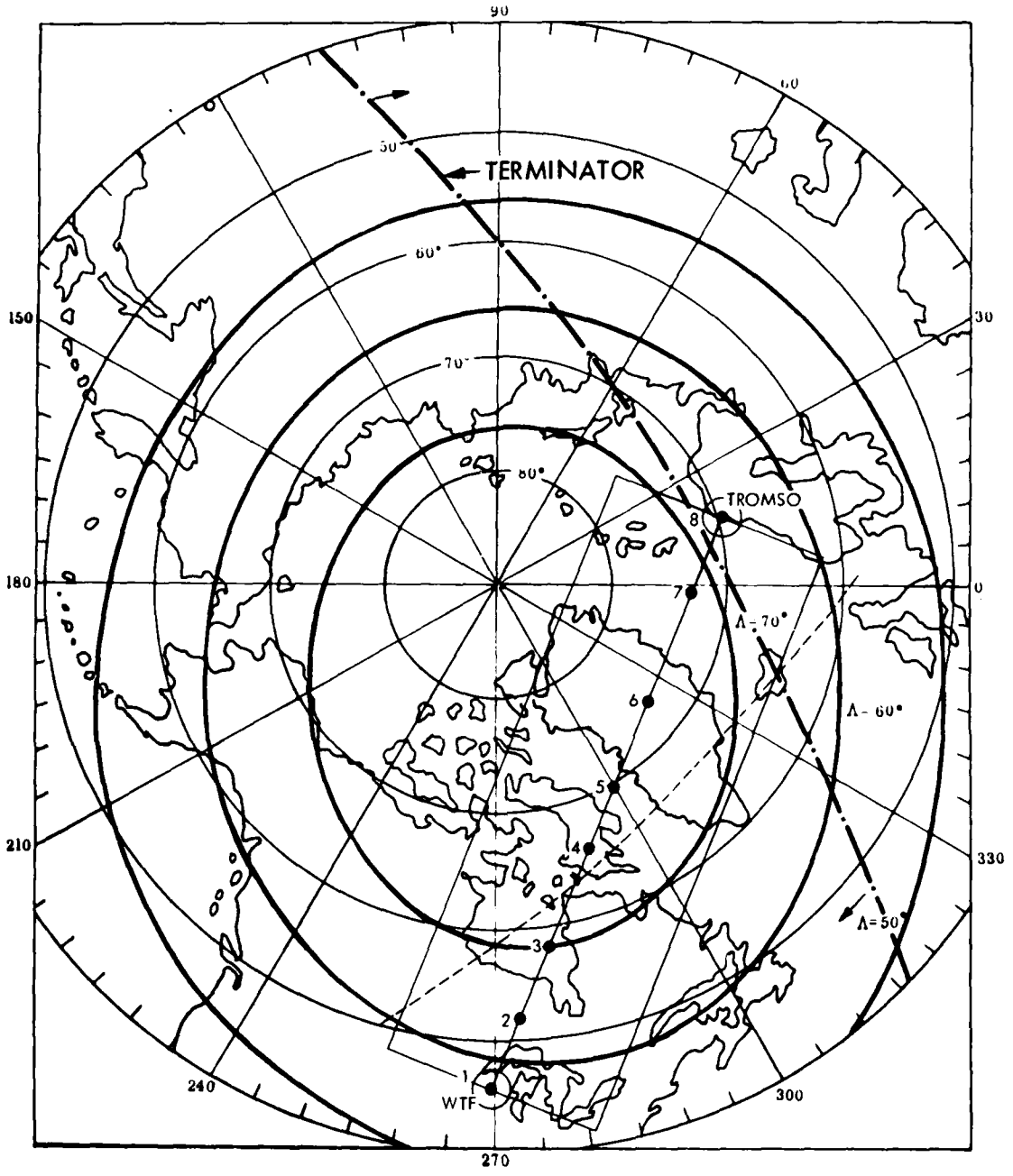

Figure 4.1. The great circle path from the Wisconsin Test Facility to Tromso is shown along with the center points of the segments. Two parallel paths separated by about 1100 km from the "direct path" are called the "north" and "south" paths. The light dashed curve is the solar terminator for local noon at 45°W longitude on 21 December. The dash-dot curve is the terminator for local noon at the longitude of Chatanika, Alaska on 4 August.

Table 4.1. Latitude and local time for the various segments of the path WTF to Tromso (calculated for midpoint of segment).† North and South paths are displaced about 1100 km from the great circle path to Tromso referred to as the 'direct' path.

Path	1	2	3	4	5	6	7	8
	Lat./ LT*							
North	48°N/0806	55°/0818	62°/0830	71°/0900	75°/0930	82°/1100	83°/1600	75°/1748
Direct	46°/0854	52°/0912	58°/0930	65°/1024	69°/1100	73°/1206	73°/1454	69°/1612
South	42°/0942	47°/1000	52°/1024	57°/1112	62°/1148	63°/1242	64°/1430	61°/1524

†Local noon occurs at 45°W. Terminator position refers to 21 December.

*LT denotes local time.

Examples of the deduced electron and ion density profiles are given in Figures 4.2 to 4.4. The profiles of all segments are listed in Tables 4.4 and 4.5. Figure 4.2 shows the calculated variation of electron density for four selected segments of the direct path. Segment 1 refers to the WTF area and the curve shows the quiet time profile calculated by the revised ion chemistry model for a local time of 0854. The model calculations cover the altitude range 80 to 50 km and are extended down to the surface using the standard ambient daytime values and up to 160 km using typical values. The other three profiles represent PCA conditions. The remaining four segment profiles fall within the range of values limited by profiles 6 and 8. For this path, covering 110^{o} in longitude or 7.3 hours of local time, the local time variations of the ionospheric chemistry resulted in N_e values being different by a factor of 10 at 40 km decreasing with altitude to a factor of 3 at 60 km and essentially no variation at 80 km. Similarly, Figure 4.3 shows the associated changes in the positive ion density. Here the major variations are found at heights between 50 and 75 km with little change above and below these altitudes.

Variations of the important ionospheric parameters occur not only along the propagation path, but also in the horizontal direction perpendicular to the path. A full 3D code should include such local time changes. To illustrate this point, Figure 4.4 shows the variation of electron and ion densities for the Greenland segment. The "north" and "south" points represent ionospheric conditions 1100 km to the north and south, respectively, of the actual propagation path over Greenland. Similar sets of profiles for the remaining 7 segments have been computed. Depending upon the actual difference in local time, changes in N_e by a factor of up to 4 have been deduced for an altitude of 60 km. The positive ion values may differ by a factor of approximately two at 60 km.

Using the deduced sets of N_e and N_+ profiles shown in Tables 4.4 and 4.5 at the end of this section the ELF field strengths for WTF to Tromso have been calculated. The results for a transmission frequency of 75 Hz are given in Table 4.2.

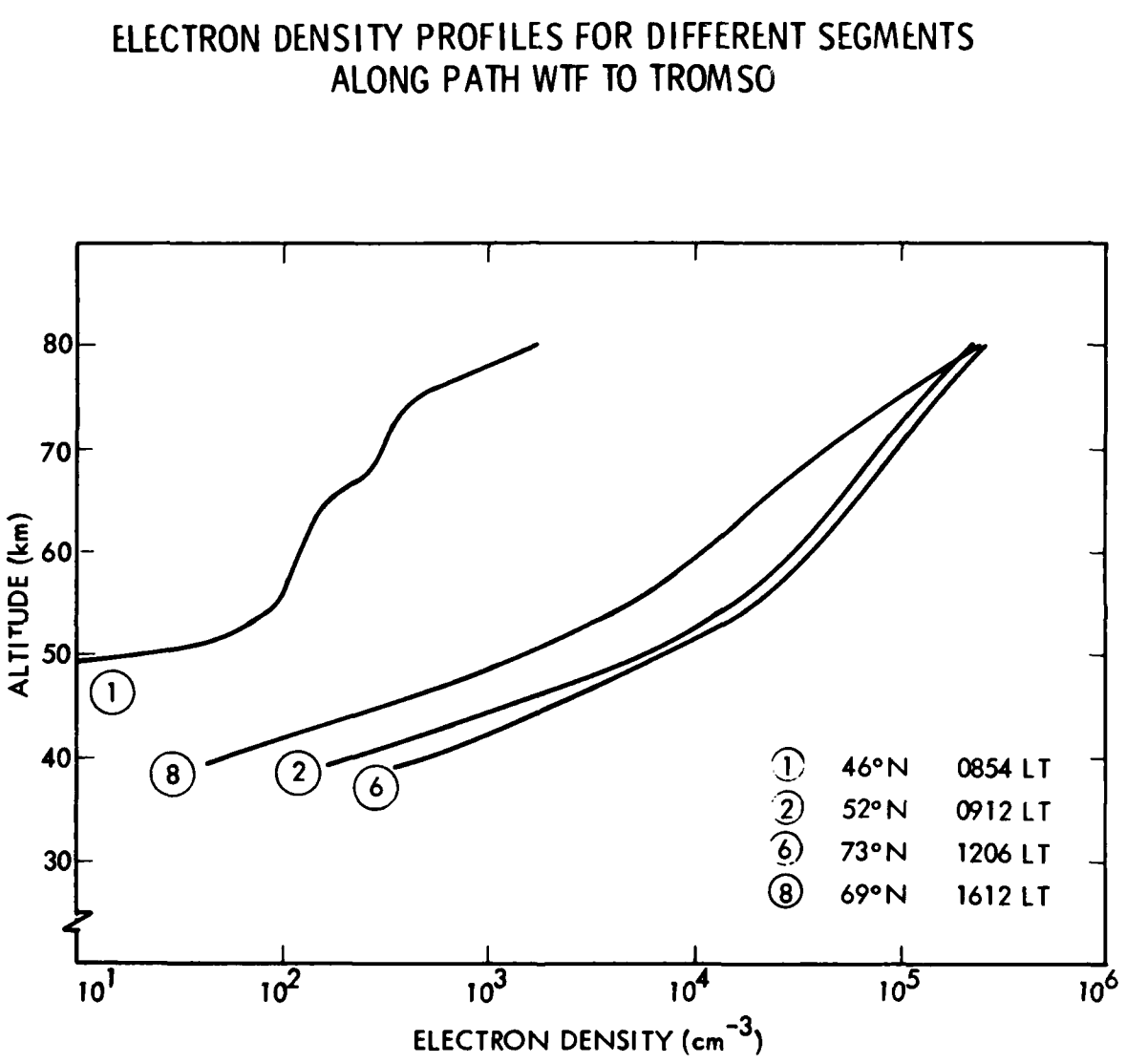

Figure 4.2. Electron density profiles for different segments along the great circle path WTF to Tromso during a simulated PCA on 21 December. The WTF segment 1 is assumed to have ambient conditions.

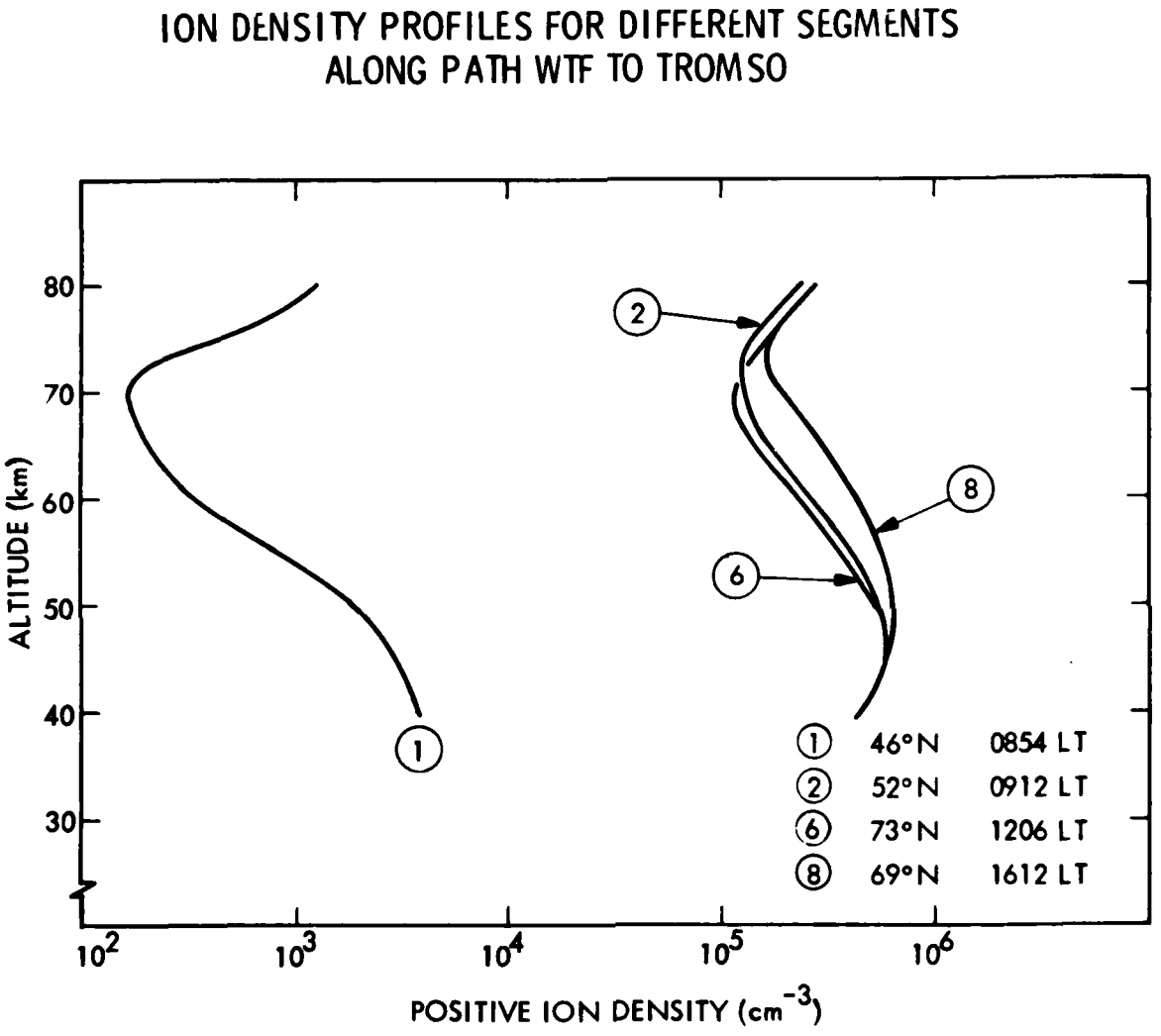

Figure 4.3. Ion density profiles for different segments along the great circle path WTF to Tromso during a simulated PCA on 21 December. The WTF segment 1 is assumed to have ambient conditions.

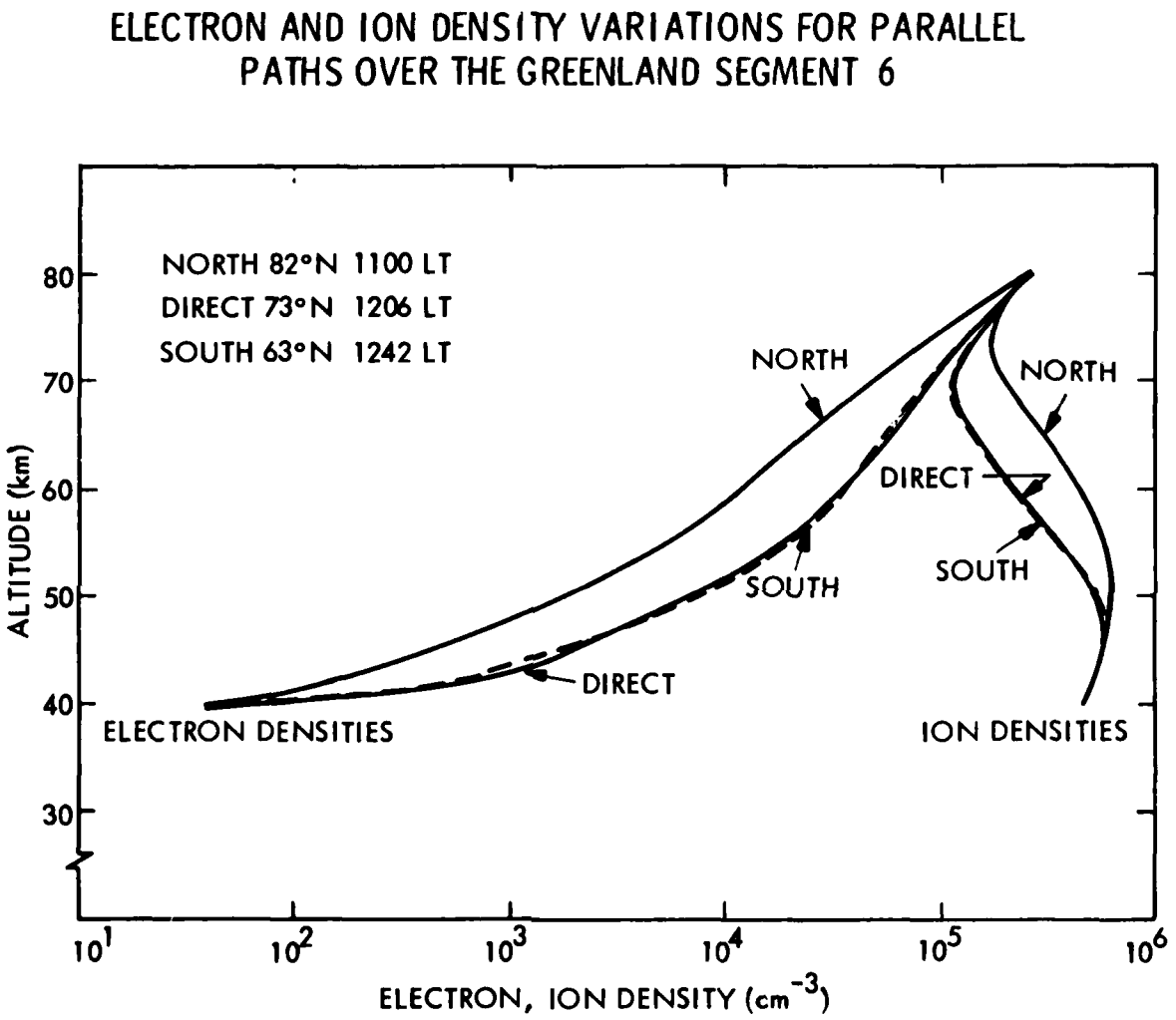

Figure 4.4. Electron and ion density profiles for segment 6, Greenland, over the three paths during a simulated PCA on 21 December.

Table 4.2 Calculations of ELF field strengths at 75 Hz for WTF to Tromso for three parallel paths. PCA conditions prevail over path except over transmitter area.

		ΔPCA-Day
Ambient day at 75 Hz	-154.7 dB	---
Direct Path	-155.9 dB	-1.2 dB
South Path	-155.4 dB	-0.7 dB
North Path	-156.4 dB	-1.7 dB

In deriving the result for ambient daytime conditions given in Table 4.2 one assumes that the quiet time N_e and N_+ profiles can be applied at all points along the propagation path. Such an approach is a reasonable first order approximation to the real situation. The results given in Table 4.3 show, however, that for more refined calculations local time variations of the ionospheric parameters are predicted and should be taken into account. The results for the three parallel paths represent calculations with different geometries of the propagation path with respect to the terminator. These sample results indicate a spread in field strength values of 1.0 dB due to the different geometries, calculated for a wintertime ionosphere (21 December).

Similar calculations over the WTF-Tromso path have been made for the actual conditions during the SPE on 4 August 1972 at the peak of the event, with the terminator in its proper position for that season as shown in Figure 4.1. It may be noted that the Tromso area is in twilight; all other segments are in daylight. The calculated profiles are given in Table 4.6 at the end of the section. The standard segmentation, ground conductivities, and magnetic fields were used.

We compare two runs both made using the ion pair production rates for the SPE of 4 August 1972, both having the WTF area in ambient conditions, both along the direct great wide path, one calculated for actual conditions on 4 August 1972 and the other for the 21 December season, with local noon at 45°W.

Table 4.3. Propagation characteristics attenuation, relative phase velocity and excitation factor, at 75 Hz calculated for the WTF transmitter area for standard ambient day as well as for 4 August and 21 December. The last two sets were derived using N_e and N_+ profiles calculated by the LMSC ion chemistry code.

Standard Ambient Day			Calculated Ambient Day For:					
			4 August			21 December		
Attn. dB/Mm	v/c	Wait Mag dB	Attn.	v/c	Wait Mag	Attn.	v/c	Wait Mag
1.37	0.82	-3.22	1.74	0.76	-0.71	1.58	0.75	-0.57

Signal Strength WTF - Tromso	
4 August 1972 SPE conditions	-156.2 dB
21 December conditions	-155.9 dB

The two runs show only a minor difference in field strength, 0.3 dB, with the winter solstice run having the higher value. This difference is, however, within the accuracy of our calculations and may not be significant.

In an earlier report on this project (Imhof et al., 1978) a calculation of propagation from WTF to Tromso was made for SPE conditions at 21 March and at a time of 2200 UT. The profiles of N_e used in the calculations were derived from the radar measurements made at chosen times during the event. The N_e values were, however, uncorrected for the presence of negative ions and were thus generally too large, in some cases by as much as a factor of two. The corresponding N_+ values were, as a result, too small. In that previous exercise the calculated signal strength at Tromso was -158.1 dB, about 2 dB weaker than the new values for SPE conditions discussed above. The larger attenuation in that case can be attributed mostly to the larger electron densities.

DISCUSSION OF AMBIENT PROFILES

In this report we have described and made use of three ambient daytime profiles. The standard profile which has been used as a reference for several years by a number of workers was discussed in Section 3. In this section we have also described ambient electron density profiles calculated by the MESTRATOS ion chemistry code for ambient conditions at the WTF latitude 46 N at two seasons and times: (1) 21 December at 0854 LT and (2) 4 August at 1542 LT. These three profiles are shown in Figure 4.5 and their propagation characteristics are given in Table 4.3. The 55 km electron densities on 21 December are larger than those on 4 August. The difference may be accounted for in terms of diurnal effects.

The choice of ambient conditions over the transmitter can make a significant difference in the results of ELF field strength calculations. For example, if

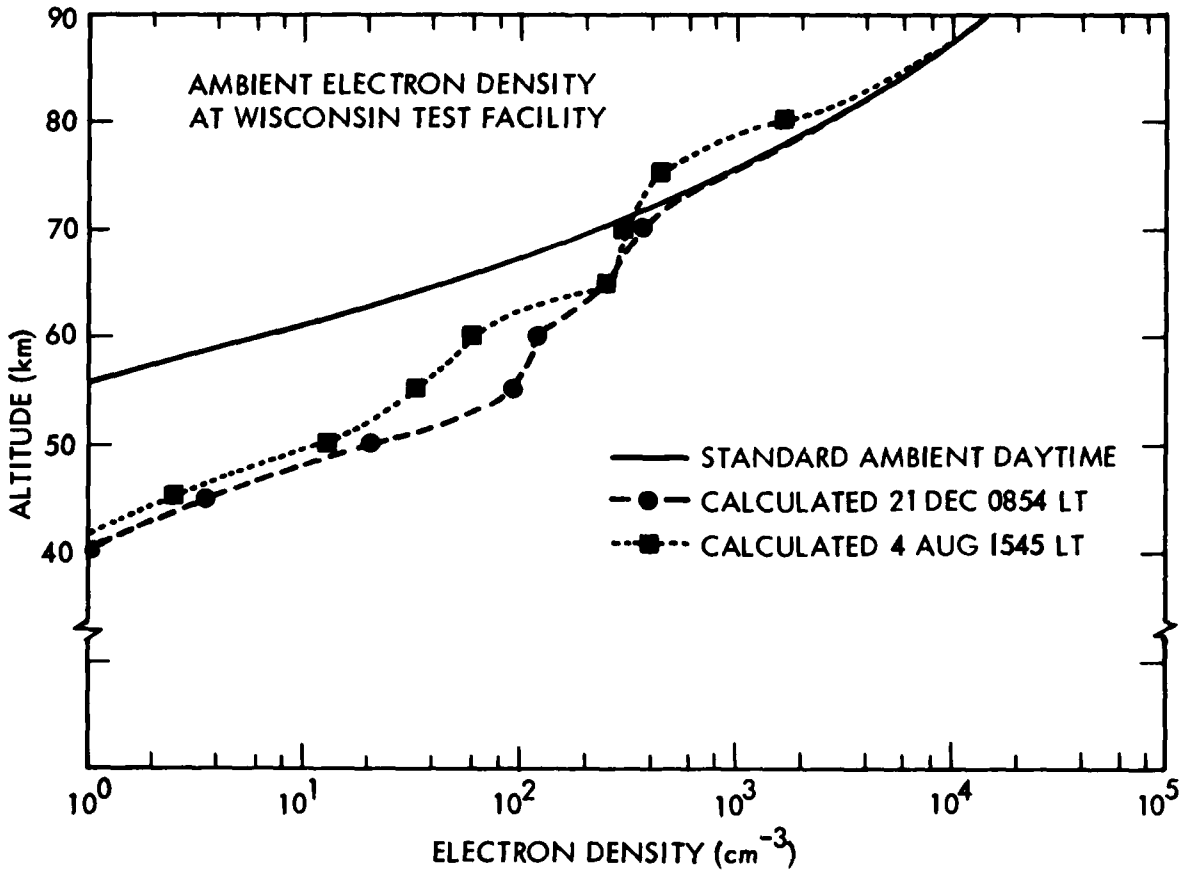

Figure 4.5. Comparison of ambient daytime electron density profiles at WTF for the two seasons and times of day with the standard ambient daytime profile discussed earlier in Section 3.

a calculation is made for the WTF to Tromso path using the actual 4 August 1972 SPE conditions, including the calculated 4 August ambient electron density profile shown in Figure 4.5 over the transmitter, the resulting absolute field strength is -156.2 dB as stated earlier in this section. If, however, the profiles over the transmitter are changed to the standard ambient daytime profiles of Section 3 and Figure 4.5 the result is -156.9 dB, 0.7 dB weaker, a significant difference.

Table 4·4. Electron and ion densities calculated for the first segment of the path WTF to Norway, i.e., the area around the WTF transmitter. Local noon occurs at 45°W and terminator position refers to 21 Dec. Values are entered for the direct, north and south paths. Conditions are assumed to be ambient at the transmitter.

Altitude (km)	Segment #1					
	Ne (cm-3)			N+ (cm-3)		
	North	Direct	South	North	Direct	South
160		1.80 (5)			1.80 (5)	
150		1.60 (5)			1.60 (5)	
140		1.50 (5)			1.50 (5)	
1.30		1.30 (5)			1.30 (5)	
120		1.10 (5)			1.10 (5)	
110		8.60 (5)			8.60 (4)	
100		6.00 (4)			6.00 (4)	
95		3.60 (4)			3.60 (4)	
90		1.50 (4)			1.50 (4)	
85		7.00 (3)			7.00 (3)	
80	2.72 (3)	2.71 (3)	2.63 (3)	2.84 (3)	2.79 (3)	2.67 (3)
75	8.97 (2)	9.30 (2)	9.08 (2)	1.04 (3)	1.02 (3)	9.64 (2)
70	2.78 (2)	3.64 (2)	3.86 (2)	4.43 (2)	4.69 (2)	4.60 (2)
65	1.72 (2)	2.56 (2)	2.78 (2)	4.74 (2)	4.39 (2)	4.52 (2)
60	1.03 (2)	1.23 (2)	9.87 (1)	7.34 (2)	3.53 (2)	2.76 (2)
55	3.45 (1)	9.48 (1)	7.48 (1)	1.41 (3)	8.48 (2)	6.35 (2)
50	8.96 (0)	2.05 (1)	3.37 (1)	2.12 (3)	1.98 (3)	1.71 (3)
45	3.17 (0)	3.58 (0)	4.69 (0)	3.08 (3)	3.05 (3)	3.03 (3)
40	1.26 (0)	1.20 (0)	1.18 (0)	4.49 (3)	4.51 (3)	4.48 (3)

NOTE: Values for the north and south paths for altitudes above 80 km are set equal to those of the direct path.

Table 4.5. Calculated electron and ion density profiles for simulated SPE on 21 December. The direct path is the great circle path from WTF to Tromso.

	Altitude (km)	N_e (cm-3)			N+ (cm-3)		
		North	Direct	South	North	Direct	South
Segment #2	80	2.22 (5)	2.29 (5)	2.39 (5)	2.29 (5)	2.36 (5)	2.44 (5)
	75	1.19 (5)	1.19 (5)	1.20 (5)	1.39 (5)	1.39 (5)	1.39 (5)
	70	7.39 (4)	7.50 (4)	7.56 (5)	1.29 (5)	1.28 (5)	1.27 (5)
	65	4.43 (4)	4.77 (4)	4.84 (4)	1.76 (5)	1.67 (5)	1.64 (5)
	60	2.46 (4)	2.86 (4)	2.92 (4)	2.81 (5)	2.58 (5)	2.53 (5)
	55	1.13 (4)	1.48 (4)	1.48 (4)	4.41 (5)	3.95 (5)	3.95 (5)
	50	4.17 (3)	5.48 (3)	5.86 (3)	5.68 (5)	5.43 (5)	5.36 (5)
	45	1.12 (3)	1.15 (3)	1.25 (3)	5.80 (5)	5.79 (5)	5.77 (5)
	40	2.38 (2)	2.30 (2)	2.18 (2)	4.67 (5)	4.67 (5)	4.68 (5)
Segment #3	80	2.39 (5)	2.44 (5)	2.59 (5)	2.44 (5)	2.50 (5)	2.63 (5)
	75	1.34 (5)	1.31 (5)	1.32 (5)	1.45 (5)	1.49 (5)	1.48 (5)
	70	8.26 (4)	8.07 (4)	8.17 (5)	1.24 (5)	1.26 (5)	1.25 (5)
	65	5.00 (4)	5.07 (4)	5.26 (4)	1.65 (5)	1.61 (5)	1.56 (5)
	60	2.55 (4)	3.02 (4)	3.24 (4)	2.66 (5)	2.46 (5)	2.35 (5)
	55	1.01 (4)	1.50 (4)	1.69 (4)	4.69 (5)	3.92 (5)	3.69 (5)
	50	3.06 (3)	5.32 (3)	6.96 (3)	5.92 (5)	5.45 (5)	5.15 (5)
	45	7.02 (2)	1.34 (3)	1.53 (3)	5.90 (5)	5.74 (5)	5.70 (5)
	40	1.01 (2)	2.82 (2)	2.31 (2)	4.70 (5)	4.66 (5)	4.67 (5)
Segment #4	80	2.40 (5)	2.52 (5)	2.68 (5)	2.53 (5)	2.57 (5)	2.71 (5)
	75	1.13 (5)	1.36 (5)	1.36 (5)	1.61 (5)	1.51 (5)	1.51 (5)
	70	4.03 (4)	8.37 (4)	8.34 (4)	2.07 (5)	1.23 (5)	1.23 (5)
	65	1.96 (4)	5.23 (4)	5.44 (4)	3.19 (5)	1.56 (5)	1.52 (5)
	60	1.02 (4)	3.19 (4)	3.41 (4)	4.47 (5)	2.38 (5)	2.26 (5)
	55	4.38 (3)	1.66 (4)	1.82 (4)	5.67 (5)	3.73 (5)	3.55 (5)
	50	1.42 (3)	5.56 (3)	7.19 (3)	6.30 (5)	5.41 (5)	5.10 (5)
	45	2.92 (2)	1.47 (3)	1.35 (3)	6.00 (5)	5.72 (5)	5.75 (5)
	40	4.06 (1)	3.03 (2)	2.58 (2)	4.72 (5)	4.66 (5)	4.67 (5)

Table 4.5, Cont'd.

	Altitude (km)	N_e (cm-3)			N+ (cm-3)		
		North	Direct	South	North	Direct	South
Segment #5	80	2.41 (5)	2.54 (5)	2.69 (5)	2.53 (5)	2.59 (5)	2.72 (5)
	75	1.19 (5)	1.39 (5)	1.39 (5)	1.58 (5)	1.51 (5)	1.52 (5)
	70	3.95 (4)	8.22 (4)	8.25 (4)	2.08 (5)	1.21 (5)	1.21 (5)
	65	2.08 (4)	5.50 (4)	5.61 (4)	3.07 (5)	1.50 (5)	1.47 (5)
	60	1.07 (4)	3.19 (4)	3.49 (4)	4.40 (5)	2.38 (5)	2.24 (5)
	55	4.73 (3)	1.58 (4)	1.88 (4)	5.60 (5)	3.82 (5)	3.52 (5)
	50	1.57 (3)	5.93 (3)	7.37 (3)	6.26 (5)	5.33 (5)	5.07 (5)
	45	2.95 (2)	1.55 (3)	1.33 (3)	6.00 (5)	5.70 (5)	5.75 (5)
	40	4.14 (1)	3.02 (2)	2.90 (2)	4.72 (5)	4.66 (5)	4.66 (5)
Segment #6	80	2.43 (5)	2.56 (5)	2.77 (5)	2.60 (5)	2.59 (5)	2.79 (5)
	75	1.08 (5)	1.48 (5)	1.47 (5)	1.66 (5)	1.55 (5)	1.58 (5)
	70	4.44 (4)	8.97 (4)	8.76 (4)	1.93 (5)	1.18 (5)	1.20 (5)
	65	2.75 (4)	5.82 (4)	5.66 (4)	2.93 (5)	1.42 (5)	1.42 (5)
	60	1.17 (4)	3.39 (4)	3.67 (4)	4.25 (5)	2.31 (5)	2.14 (5)
	55	5.40 (3)	1.98 (4)	1.99 (4)	5.47 (5)	3.42 (5)	3.38 (5)
	50	1.68 (3)	6.72 (3)	7.16 (3)	6.24 (5)	5.20 (5)	5.11 (5)
	45	3.70 (2)	2.01 (3)	1.67 (3)	5.98 (5)	5.59 (5)	5.67 (5)
	40	5.11 (1)	3.81 (3)	3.73 (2)	4.72 (5)	4.64 (5)	4.64 (5)
Segment #7	80	2.43 (5)	2.39 (5)	2.80 (5)	2.60 (5)	2.55 (5)	2.82 (5)
	75	1.18 (5)	1.08 (5)	1.46 (5)	1.66 (5)	1.66 (5)	1.57 (5)
	70	4.44 (4)	4.48 (5)	8.72 (4)	1.93 (5)	1.94 (5)	1.20 (5)
	65	2.25 (4)	2.25 (4)	5.81 (4)	2.93 (5)	2.92 (5)	1.44 (5)
	60	1.17 (4)	1.16 (4)	3.54 (4)	4.25 (5)	4.23 (5)	2.22 (5)
	55	5.40 (3)	5.37 (3)	1.82 (4)	5.47 (5)	5.45 (5)	3.61 (5)
	50	1.68 (3)	1.68 (3)	6.55 (3)	6.24 (5)	6.23 (5)	5.24 (5)
	45	3.70 (2)	3.69 (2)	1.74 (3)	5.98 (5)	5.98 (5)	5.66 (5)
	40	5.11 (1)	5.09 (1)	3.68 (2)	4.72 (5)	4.72 (5)	4.64 (5)
Segment #8	80	2.38 (5)	2.35 (5)	2.76 (5)	2.51 (5)	2.51 (5)	2.79 (5)
	75	1.16 (5)	1.00 (5)	1.39 (5)	1.60 (5)	1.67 (5)	1.51 (5)
	70	4.24 (5)	4.23 (4)	8.52 (4)	2.00 (5)	1.99 (5)	1.21 (5)
	65	2.13 (4)	2.11 (4)	5.51 (4)	3.03 (5)	3.03 (5)	1.48 (5)
	60	1.08 (4)	1.08 (4)	3.35 (4)	4.37 (5)	4.36 (5)	2.34 (5)
	55	4.86 (3)	4.85 (3)	1.68 (4)	5.57 (5)	5.57 (5)	3.73 (5)
	50	1.54 (3)	1.54 (3)	5.94 (3)	6.27 (5)	6.26 (5)	5.31 (5)
	45	3.42 (2)	3.41 (2)	1.42 (3)	5.99 (5)	5.98 (5)	5.72 (5)
	40	4.78 (1)	4.76 (1)	2.57 (2)	4.72 (5)	4.72 (5)	4.67 (5)

actual SPE of August 1972. The path is the great circle from WTF to Tromso.

	Altitude (km)	N_e (cm-3)	N_+ (cm-3)		Altitude (km)	N_e (cm-3)	N_+ (cm-3)
Segment #1	80	2.02 (3)	2.03 (3)	Segment #5	80	1.26 (5)	1.34 (5)
	75	6.11 (2)	7.11 (2)		75	8.75 (4)	1.18 (5)
	70	3.47 (2)	5.41 (2)		70	5.71 (4)	1.42 (5)
	65	2.54 (2)	7.91 (2)		65	3.48 (4)	2.11 (5)
	60	6.11 (1)	5.70 (2)		60	1.91 (4)	3.33 (5)
	55	3.45 (1)	1.24 (3)		55	8.76 (3)	4.84 (5)
	50	1.31 (1)	2.25 (3)		50	2.86 (3)	5.97 (5)
	45	3.16 (0)	3.43 (3)		45	6.17 (2)	5.92 (5)
	40	0.87 (0)	4.91 (3)		40	1.19 (2)	4.70 (5)
Segment #2	80	1.39 (5)	1.45 (5)	Segment #6	80	1.24 (5)	1.32 (5)
	75	9.23 (4)	1.16 (5)		75	8.63 (4)	1.19 (5)
	70	6.20 (4)	1.31 (5)		70	5.57 (4)	1.45 (5)
	65	3.81 (4)	1.95 (5)		65	3.40 (4)	2.16 (5)
	60	2.17 (4)	3.08 (5)		60	1.88 (4)	3.37 (5)
	55	9.38 (3)	4.74 (5)		55	8.62 (3)	4.87 (5)
	50	3.15 (3)	5.91 (5)		50	2.78 (3)	5.99 (5)
	45	6.64 (2)	5.91 (5)		45	6.11 (3)	5.92 (5)
	40	1.19 (2)	4.70 (5)		40	1.21 (3)	4.70 (5)
Segment #3	80	1.32 (5)	1.38 (5)	Segment #7	80	1.24 (5)	1.33 (5)
	75	9.00 (4)	1.15 (5)		75	8.57 (4)	1.21 (5)
	70	6.04 (4)	1.34 (5)		70	5.43 (4)	1.49 (5)
	65	3.70 (4)	2.01 (5)		65	3.26 (4)	2.23 (5)
	60	2.01 (4)	3.23 (5)		60	1.76 (4)	3.47 (5)
	55	9.10 (3)	4.79 (5)		55	7.60 (3)	5.03 (5)
	50	3.03 (3)	5.94 (5)		50	2.32 (3)	6.09 (5)
	45	6.42 (2)	5.92 (5)		45	6.24 (2)	5.92 (5)
	40	1.17 (2)	4.70 (5)		40	1.28 (2)	4.70 (5)
Segment #4	80	1.29 (5)	1.36 (5)	Segment #8	80	1.23 (5)	1.32 (5)
	75	8.85 (4)	1.18 (5)		75	8.52 (4)	1.20 (5)
	70	5.82 (4)	1.40 (5)		70	5.37 (4)	1.54 (5)
	65	3.51 (4)	2.09 (5)		65	3.08 (4)	2.36 (5)
	60	1.92 (4)	3.31 (5)		60	1.57 (4)	3.73 (5)
	55	8.92 (3)	4.80 (5)		55	6.71 (3)	5.20 (5)
	50	2.28 (3)	5.96 (5)		50	2.31 (3)	6.10 (5)
	45	6.18 (2)	5.92 (5)		45	5.74 (2)	5.94 (5)
	40	1.18 (2)	4.70 (5)		40	9.39 (1)	4.71 (5)

Section 5
CRITERIA FOR INITIATING EXPERIMENTAL MEASUREMENTS DURING AN ELF-PCA FIELD PROGRAM

5.1 CRITERION FOR SELECTION OF A SUITABLE PCA

In the proposed NRL ELF-PCA field program measurements will be made of the field strengths of ELF signals propagating across the polar cap during disturbed conditions in a PCA event. The signal strength measurements are to be compared with ELF propagation code predictions. The ion and electron conductivity altitude profiles which are necessary inputs to the ELF codes will be obtained by making use of satellite measurements of the precipitating proton fluxes and energy spectra. The proton inputs can be used in a proton energy deposition code to find ion pair production rate profiles throughout the atmosphere. Present ion chemistry codes permit the determination of ion and electron densities, and hence conductivities, down to about 50 km with reasonable accuracy. Because of uncertainties in the ion chemistry below 50 km, simultaneous balloon measurements of ion and electron conductivities up to about 40 km would be highly desirable.

It is necessary to be able to establish in real time whether a PCA event is of sufficient intensity to make it worhtwhile to initiate the measurement program. The method suggested here involves the use of the satellite proton flux measurements at an energy of about 70 MeV for which most of the ion pair production occurs near 40 km. In the following analysis estimates are made of a suitable minimum flux criterion.

First the ion densities at 40 km for ion pair production rates, q, of $1x10^3$, $5x10^3$, $1x10^4$, and $5x10^4$ $cm^{-3}sec^{-1}$ are calculated as indicated in Table 5.1.

Table 5.1. Ion densities and field strengths for various ion production rates at 40 km.

h (km)	q (ion pairs $cm^{-3}s^{-1}$)	α_i cm^3s^{-1}	$N_+(40km) \approx \sqrt{q/\alpha_i}$ (cm^{-3})	Field Strength (75 Hz) WTF-Tromso
40	1.00 (3)	6.84 (-8)	1.21 (5)	-158.0 db
40	5.00 (3)	6.84 (-8)	2.70 (5)	-158.8 db
40	1.00 (4)	6.84 (-8)	3.82 (5)	-159.2 db
40	5.00 (4)	6.84 (-8)	8.55 (5)	-160.0 db

The value of the neutralization rate used in these calculations is taken from Table 3.7 in Imhof et al. (1978). The field strengths are obtained from Figure 5.1 which is essentially a plot of field strengths at Tromso from the WTF transmitter versus ion density at 40 km for the three PCA Day cases described in Section 2 and for the standard ambient daytime case described in Section 3. The broken line in the figure represents a fit to these data. The points on that line corresponding to the ion densities of Table 5.1, calculated for q values from $1x10^5$ to 5×10^4 $cm^{-3}s^{-1}$, are used to obtain the signal strengths shown in the table. These signal strengths for disturbed conditions represent significant departures from ambient signal strengths and are associated with q values at 40 km of the magnitude found in several representative PCA events of two recent solar cycles as shown in Figure 5.2. A reasonable criterion for a PCA of suitable intensity appears to be one producing an ion pair production rate of 1×10^3 $cm^{-3}sec^{-1}$ at 40 km, corresponding to a differential flux of 70 MeV protons at the satellite of about 3.4 particles/cm^2-sec-sr-MeV.

Caution should be exercised when using these estimates. The attenuation and excitation of the ELF waves depend on the complete N_+ and N_e profiles. The simplification of taking only the N_+ value at 40 km is clearly a major one. This procedure may, however, be a useful guideline in deciding when to start experiments during a PCA-ELF field program. It should, perhaps, not be the only criterion; multifrequency riometer observations, VLF phase deviations, and real-time satellite observations of larger portions of the proton spectrum would be valuable additions.

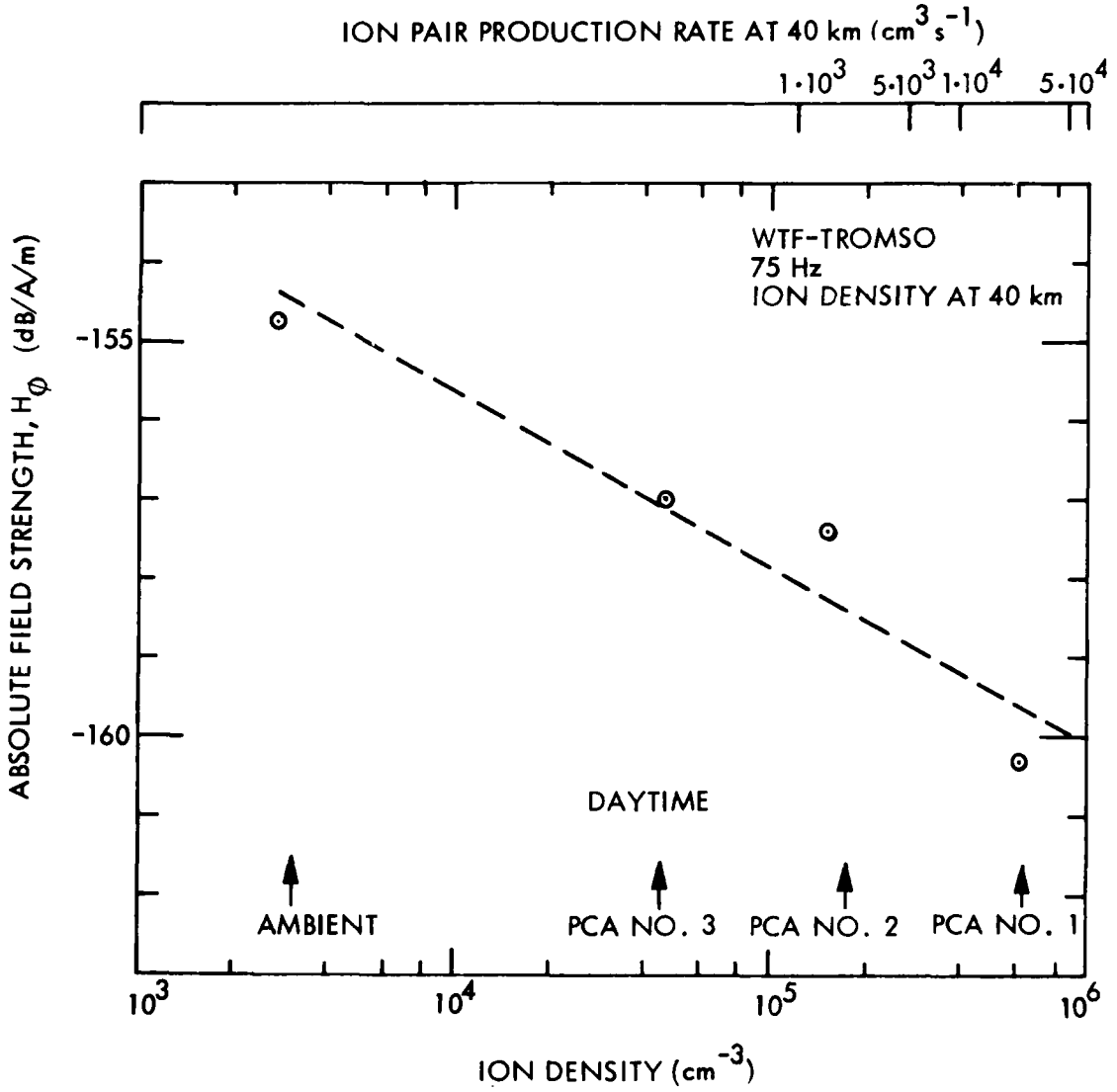

Figure 5.1. Absolute field strength for the WTF to Tromso path versus ion density at 40 km altitude for the three PCA daytime test cases (Section 2) and the standard ambient daytime profile (Section 3). Ion pair production rate at 40 km versus ion density is shown in the scale at the top of the figure.

To summarize: Guided by the ELF calculations of predicted signal strengths in Tromso we conclude that a desirable event for an ELF field program would have production rates at 40 km equal to or larger than 1×10^3 ion pairs $cm^{-3}s^{-1}$. The ELF calculations, assuming that the PCA extends over the complete path (except over the transmitter), indicate that a 3 dB or larger reduction in signal strength would occur for such an event. From Figure 5.2 which shows the ion-pair production rates for a number of PCA's, one finds that the above criterion is fulfilled for all but one of the major PCA's observed in solar cycles 19 and 20.

These estimates are based on ELF computations assuming no local time variations along the propagation path. More theoretical computation of these local time ionospheric effects should be made to substantiate whether or not the findings using this more simplified approach are still valid.

5.2 INFLUENCE OF ELF NOISE MEASUREMENTS

Figure 5.3 shows the absolute rms field strength levels of the noise at 75 Hz for 10 days in October/November 1969. A marked diurnal variation in the noise levels of 4 - 8 dB is noticed. Larsen(1974b) has shown that this variation qualitatively follows the statistics for world-wide thunderstorm activity (U.S. Air Force/Geophysics Research Directorate 1960) and reflects in gross the contribution from the three large thunderstorm areas: Asia, Africa, and America, which are most active at approximately 08, 14, and 20 hours UT, respectively.

An ELF field program conducted for night conditions (e.g., 00-06 hours UT interval) will experience lower background ELF noise as compared to a daytime experiment at times 12 - 20 hours UT. Such noise differences may be of great importance.

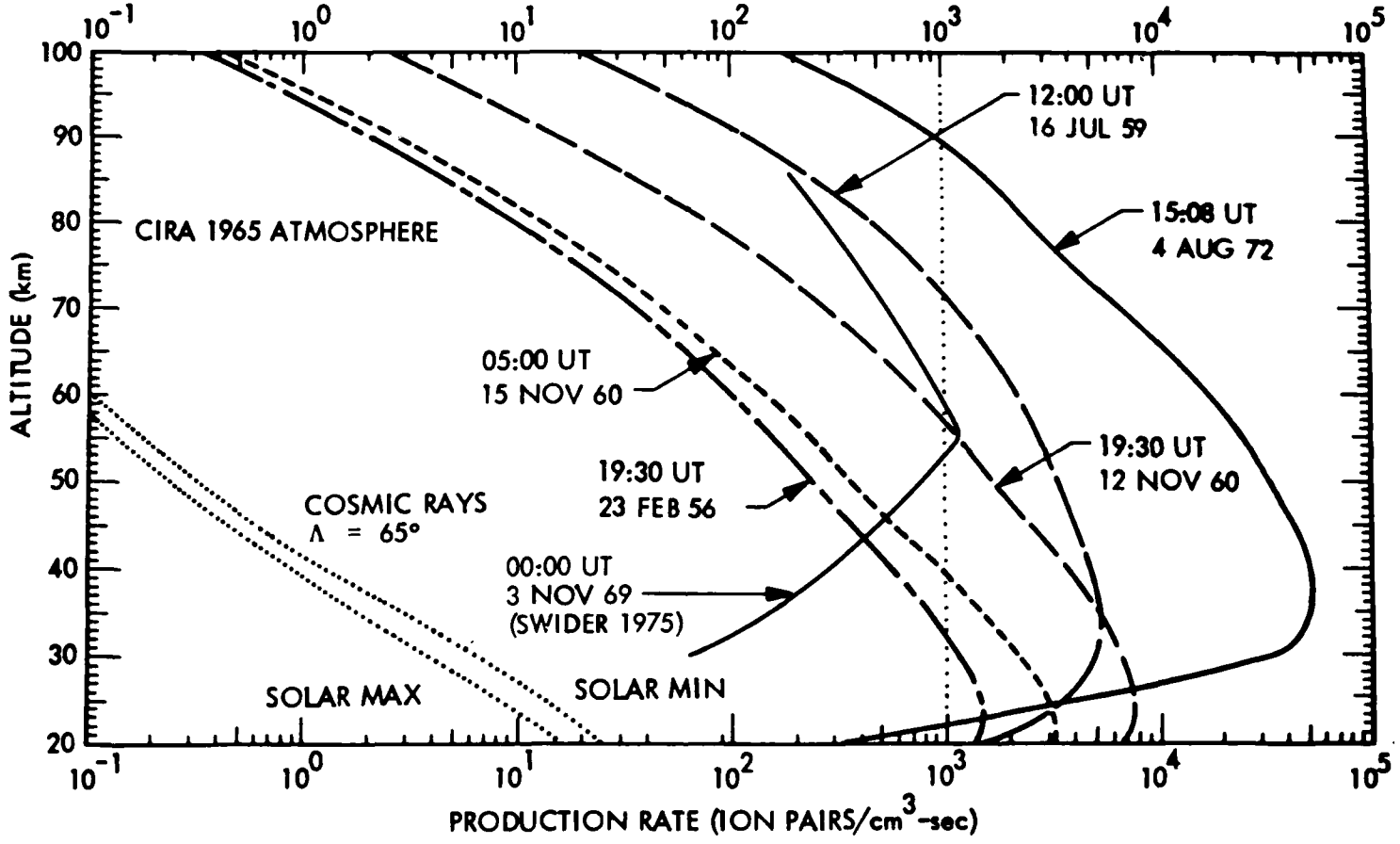

Figure 5.2 Solar proton induced ion production rates during the major solar particle events in solar cycles 19 and 20. The cosmic ray ionization for solar maximum and minimum is shown for comparison. The 4 August 1972 SPE dominates in ion production rate over all of the other events in cycles 19 and 20 at altitudes above 26 km. The dotted line shows that the criterion of a production rate at 40 km of 10^3 ion pairs/cm^3-sec would include four of the six solar particle events shown.

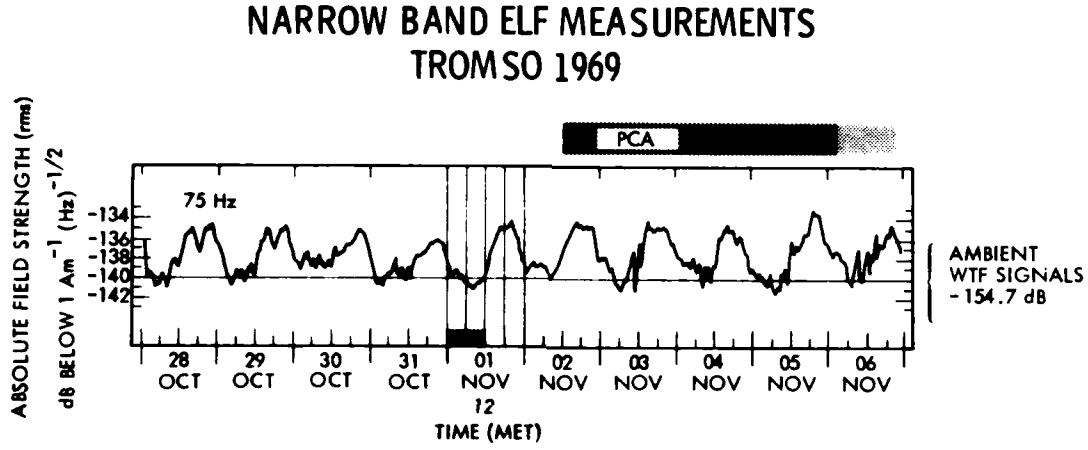

Figure 5.3. Narrow band ELF noise measurements at a frequency of 75 Hz at Tromso. The strong PCA event that started on 2 November does not seem to have a significant influence on the measured noise levels. A horizontal line shows the level of the signal strength at Tromso from the WTF transmitter for standard ambient (day or night) conditions over the path. Note that UT time is MET-1.

5.3 DATES AND TIMES FOR HAVING THE WTF-TROMSO PATH IN TOTAL DAYLIGHT OR TOTAL DARKNESS

It may be desirable to simplify the experimental analysis by having the WTF to Tromso path totally in daylight or totally in darkness, i.e., having the terminator outside the great circle path on the ground. By doing this the more difficult problem of modeling twilight in the ion chemistry can be totally or largely avoided. In Figures 5.4 and 5.5 and in Tables 5.2 and 5.3 the times for total daylight and total darkness are shown for all seasons of the year.

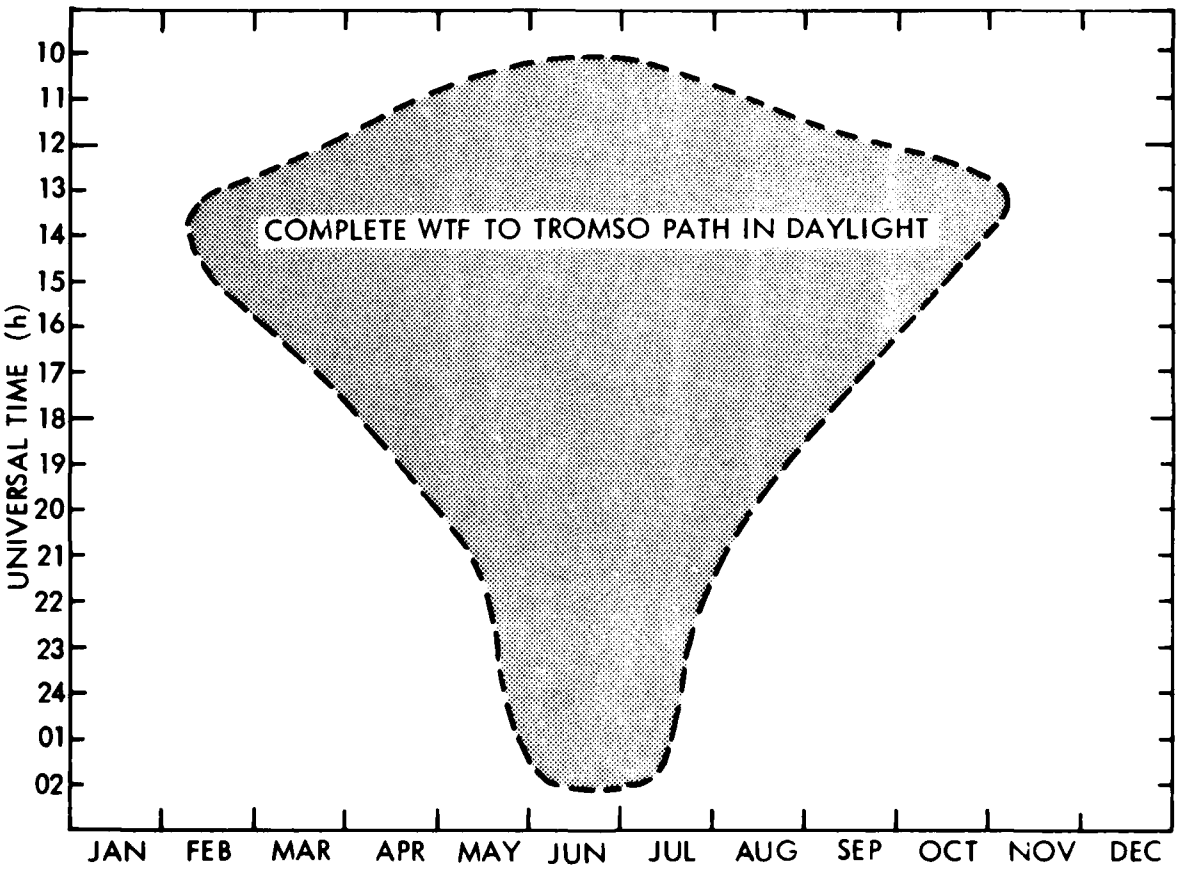

Figure 5.4. Times for which the complete WTF to Tromso path is daylight versus season.

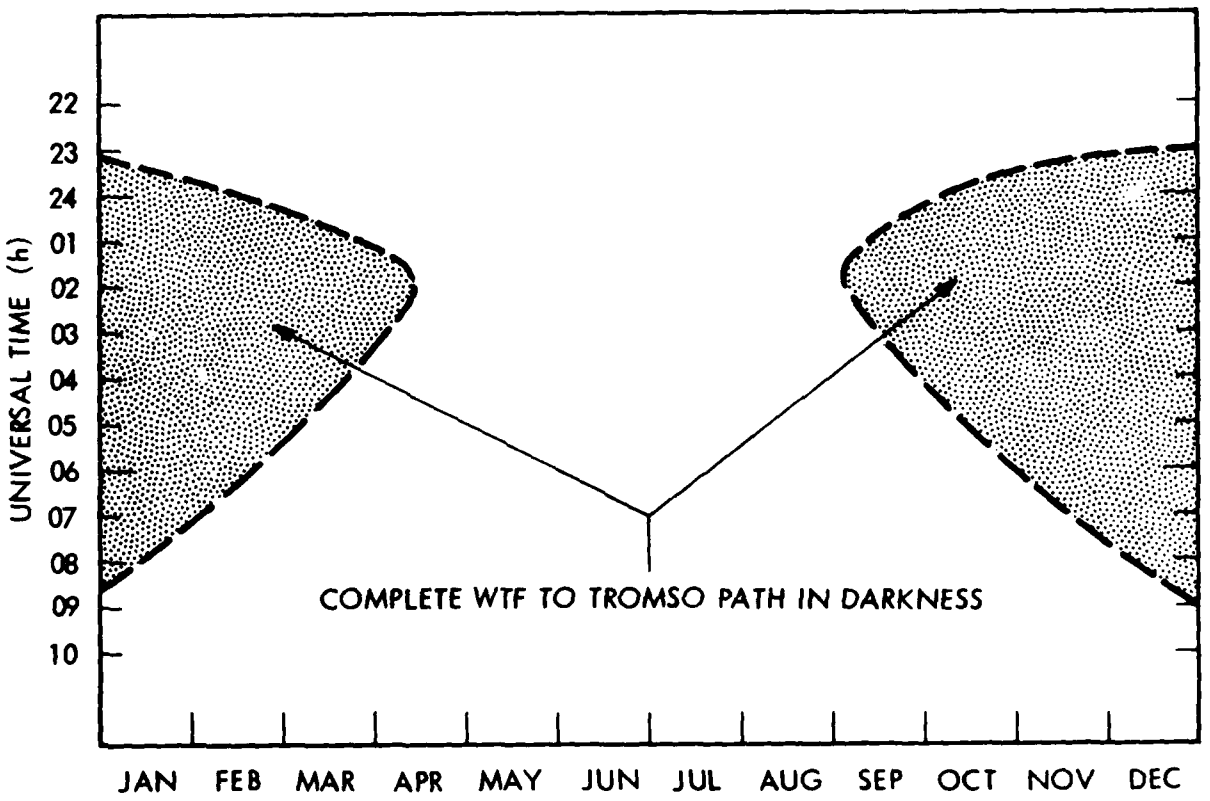

Figure 5.5 Times for which the complete WTF to Tromso path is in darkness versus season.

Table 5.2. Approximate times for WTF-Tromso path completely in daylight.

EPOCH	PATH IN DAYLIGHT UNIVERSAL TIME	CENTRAL STANDARD TIME(WTF)	APPROXIMATE DURATION (hrs)
11 Jan.	Never completely in daylight.		
25 Jan.	Never completely in daylight.		
18 Feb.	1300 - 1500	0700 - 0900	2.0
10 Mar.	1230 - 1630	0630 - 1030	4.0
24 Mar.	1200 - 1730	0600 - 1130	5.5
7 Apr.	1130 - 1830	0530 - 1230	7.0
21 Apr.	1100 - 1930	0500 - 1330	8.5
5 May	1030 - 2030	0430 - 1430	10.5
21 May	1030 - 2300	0430 - 1700	12.5
10 June	1000 - 0200	0400 - 2000	16.0
22 June	1000 - 0200	0400 - 2000	16.0
13 July	1030 - 0200	0430 - 2000	15.5
31 July	1030 - 2130	0430 - 1530	11.0
13 Aug.	1100 - 2000	0500 - 1400	9.0
24 Aug.	1100 - 1900	0500 - 1300	8.0
3 Sept.	1130 - 1830	0530 - 1230	7.0
13 Sept.	1130 - 1730	0530 - 1130	6.0
22 Sept.	1200 - 1700	0600 - 1100	5.0
1 Oct.	1200 - 1600	0600 - 1000	4.0
12 Oct.	1200 - 1530	0600 - 0930	3.5
23 Oct.	1230 - 1430	0630 - 0830	2.0
4 Nov.	1230 - 1330	0630 - 0730	1.0
18 Nov.	Never completely in daylight.		
3 Dec.	Never completely in daylight.		
21 Dec.	Never completely in daylight.		

Table 5.3. Approximate times for WTF-Tromso path in total darkness.

EPOCH	PATH IN DARKNESS		APPROXIMATE DURATION (hrs)
	UNIVERSAL TIME	CENTRAL STANDARD TIME(WTF)	
11 Jan.	2330 - 0800	1730 - 0200	8.5
25 Jan.	2330 - 0730	1730 - 0130	8.0
18 Feb.	2400 - 0600	1800 - 2400	6.6
10 Mar.	0030 - 0430	1830 - 2230	4.0
24 Mar.	0100 - 0330	1900 - 2130	2.5
7 Apr.	0130 - 0230	1930 - 2030	1.0
21 Apr.	Never in complete night.		
5 May	Never in complete night.		
21 May	Never in complete night.		
10 June	Never in complete night.		
22 June	Never in complete night.		
13 July	Never in complete night.		
31 July	Never in complete night.		
13 Aug.	Never in complete night.		
24 Aug.	Never in complete night.		
3 Sept.	0130 - 0200	1930 - 2000	0.5
13 Sept.	0100 - 0230	1900 - 2030	1.5
22 Sept.	0030 - 0330	1830 - 2130	3.0
1 Oct.	2400 - 0400	1800 - 2200	4.0
12 Oct.	2400 - 0430	1800 - 2230	4.5
23 Oct.	2330 - 0530	1730 - 2330	6.0
4 Nov.	2330 - 0600	1730 - 2400	6.5
18 Nov.	2300 - 0700	1700 - 0100	8.0
3 Dec.	2300 - 0800	1700 - 0200	9.0
21 Dec.	2300 - 0830	1700 - 0230	9.5

Section 6
THE EFFECT OF SPORADIC E-LAYERS OVER THE WTF-TROMSO PATH

Sporadic E-layers occur with sufficient frequency that they must be considered in planning an ELF-PCA field program. The occurrence of E_s layers is often 30 - 50% at specific times of day and varies with season. Thus an appreciable effect might be expected on an operational ELF system.

Three sample runs have been made with the profile measured by Voss (private communication, 1977) which has been used in previous work (e.g., Imhof et al., 1978). In this profile the E_s layer is located at an altitude of 118 km as shown in Figure 6.1. In each of these runs the standard ambient night conditions were used over all segments except one. The results are as follows:

E_s over Norwegian Sea - ambient night elsewhere - 156.5 dB
E_s over Greenland - ambient night elsewhere - 155.5 dB
E_s over Tromso area - ambient night elsewhere - 155.6 dB

These field strength values calculated for 75 Hz are of the order 1 - 2 dB lower than the ambient night value of -154.7 dB.

Table 6.1 contains the calculated attenuation rates and excitation factors for this case. The ambient night values are included for comparison. Note that the attenuation rate increases markedly for the last two segments over the Norwegian Sea and Tromso, whereas the excitation factor is rather constant for all segments.

Several authors (Davis, 1974; Barr, 1977; Pappert and Shockey, 1977, 1978) have also made calculations regarding the influence of sporadic E-layers. The latter authors present one physical explanation for the enhanced absorption in terms of an attenuation resonance between waves reflected from "normal" E-

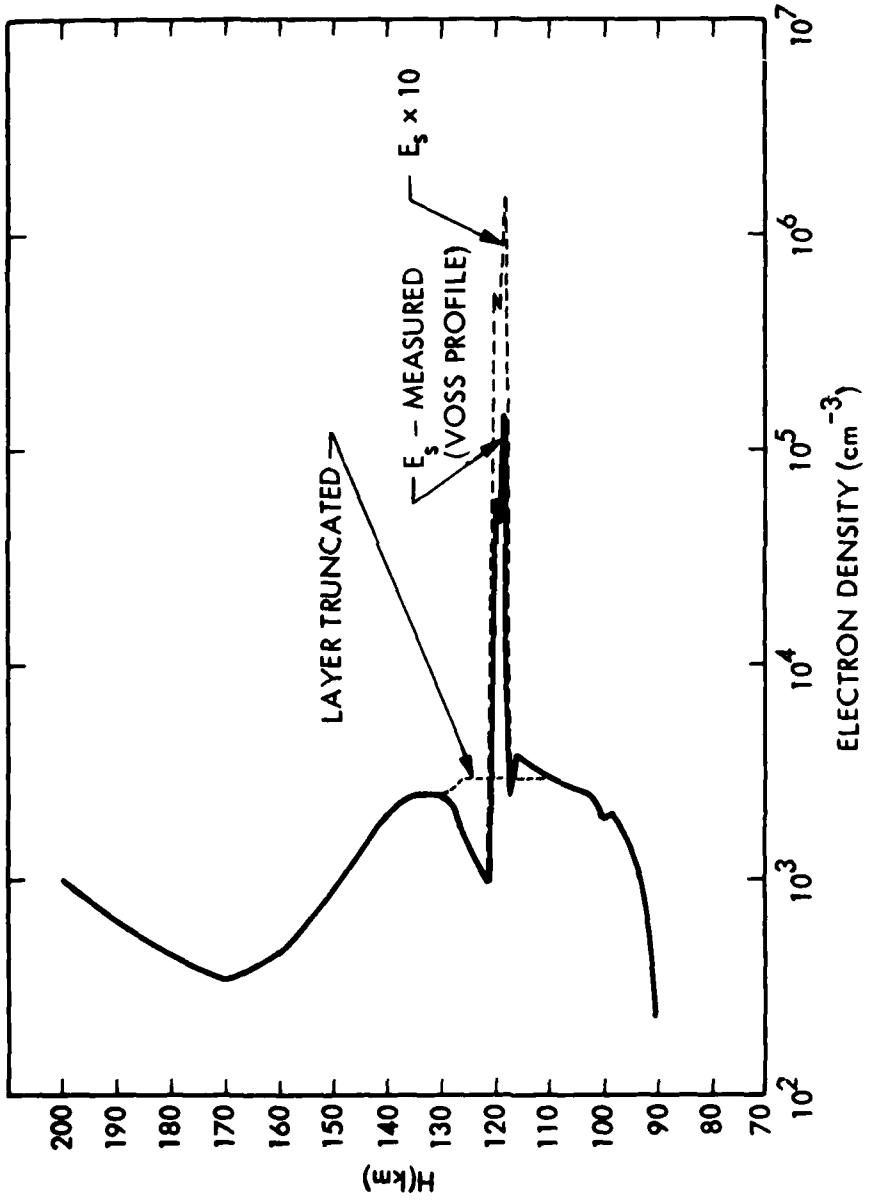

Figure 6.1. Sporadic E-layer profiles used in calculations based on the same measurements of Voss (1977). Variations of the original profile include increase of the spike by a factor of 10 and truncation of the profile as shown.

TABLE 6·1. ELF Propagation Characteristics Attenuation and Excitation Factor at 75 Hz for Ambient Night and Sporadic E Conditions Calculated for the Path WTF to Tromso.

Segment		Ambient Night		Voss E_s Profile at 118 km		Voss E_s Peak X10 at 118 km		Truncated Voss E_s Profile	
		Atten. db/Mm.	Excit. Fac.dB	Atten. dB/M_m.	Excit. Fac.	Atten. dB/Mm.	Excit. Fac.	Atten. dB/M_m.	Excit. Fac.
1	WTF Area	1.09	-5.46	1.68	-3.82	3.38	-2.00	1.99	-4.70
2	Canada	1.04	-5.52	1.49	-3.90	2.48	-2.35	1.87	-4.67
3	Hudson Bay	0.97	-5.59	1.41	-3.96	2.34	-2.42	1.80	-4.72
4	N. Canada	1.03	-5.51	1.57	-3.86	2.97	-2.13	1.92	-4.71
5	Davis Strait	0.95	-5.58	1.59	-3.89	3.49	-1.97	1.90	-4.82
6	Greenland	1.64	-4.91	2.43	-3.32	6.18	-1.31	2.58	-4.32
7	Norweg. Sea	0.90	-5.55	2.13	-3.77	8.31	-2.18	2.00	-5.11
8	Tromso Area	0.96	-5.49	2.28	-3.72	8.54	-2.67	2.06	-5.08

region heights and from the E_s layer. Especially enhanced attenuation occurs if the distance apart and thickness of these reflecting layers equal one-quarter of the local ELF wavelength in the medium.

In our earlier calculations applying the E_s profile to the WTF-Connecticut path we also predicted decreases in expected signal strength during such conditions (Imhof et al, 1976, 1977, 1978). Our results indicate that the field strength is sensitive to the height of the E_s-layer, its thickness and electron density. Variations in these parameters will cause the signal strength to vary at the receiver.

Further calculations were made as shown in Figure 6.1. In the first, the Voss E_s-layer densities were increased by a factor of 10. The waveguide characteristics are shown in Table 6.1. When this profile was used in the Norwegian Sea segment with standard ambient night elsewhere the ELF signal strength at Tromso was -165.8 dB, some 9 dB weaker than the value for the original Voss profile and 11 dB weaker than the standard ambient night result.

In a further numerical experiment the Voss peak was truncated as indicated in Figure 6.1 and when the resulting profile was used in the Norwegian Sea segment the signal strength was -160.2 dB, i.e., some 3.7 dB weaker than the Voss profile result. The ELF propagation characteristics are given in Table 6.1. The added electrons between 120 and 130 km are evidently having a major effect on the excitation factor.

These calculations suggest that more accurate calculations of the influence of E_s ought to be undertaken using actual measured profiles for areas of special interest.

Section 7
ION CHEMISTRY MODEL IMPROVEMENT

7.1 INTRODUCTION

A good ion chemistry model is a necessary element in the study of ELF propagation during solar particle events. Modeled ion and electron density profiles when used in ELF propagation codes permit the estimation of signal strengths during disturbed conditions. Such a model has been developed based on measurements made during the intense solar particle events of August 1972 (SPE72) and of November 1969 (PCA69).

During the very intense events of 3 through 11 August 1972 simultaneous observations were made with the Lockheed experiment on the polar-orbiting satellite 1971-089A and the Stanford Research Institute incoherent-scatter radar at Chatanika, Alaska (Reagan and Watt, 1976). Particle precipitation rates measured with the satellite instrumentation were used to obtain altitude profiles of ion pair production rates, Q, at 28 times, covering a solar zenith angle range of 50 to 98.6°. Corresponding measurements of electron density, N_e, were obtained from the radar measurements at the same times. These results, obtained principally between 4 and 6 August, are sufficiently extensive and contiguous in time to permit a detailed study of the diurnal behavior of the polar D-region ionosphere and neutral atmosphere during an intense solar particle event. The less intense event of 2 - 4 November, 1969 was comprehensively documented (Ulwick, 1972) and a number of good N_e, Q pairs of measurements are available for use (Swider et al., 1978).

Two of the principal variables affecting electron loss rates in the D-region and upper stratosphere, the altitude regime of greatest importance for ELF communications, are thought to be the atomic oxygen density, O (suggested, e.g., by Keneshea and Swider, 1972), and the $O_2(^1\Delta)$ density because of their important role in the negative ion chemistry. Densities of these oxygen species depend on

solar zenith angle, water concentration, ion production rate, ion production integrated over time, and on other minor species. In addition, electron loss depends on atmospheric density and temperature which may in fact be altered by the solar particle event itself, and on winds. Unfortunately, none of these variables were measured in detail during SPE72.

The diurnal, seasonal, and geographical variations of minor species, such as O and $O_2(^1\Delta)$, are thus important. Because of a lack of experimental data for these species, diurnal models for computing these species theoretically have been developed. One part of the model computes diurnal variations of a set of photodissociation and photodetachment coefficients. A second model using these coefficients computes the neutral species of interest. A third semi-empirical, simplified diurnal ion-chemistry model coupled to the neutral model calculates electron and ion densities and loss rates. The validity of the overall model is to be judged by comparison of computed and experimental electron densities. Near 80-km altitude, the large daytime values of the electron loss rate $\Psi = Q/N_e^2$ obtained in SPE72 were consistent with the dominant ions being the hydrated ions H_3O^+ (AMU = 19) and $H_3O^+ \cdot O$ (AMU = 37). This result was in sharp contrast with the PCA69 results in which the hydrated ions were not present above 73-km altitude in the daytime. A strong seasonal dependence in the effective electron loss rates under disturbed conditions is thus evident.

After a preliminary ion chemistry model was developed for solar particle events (Gunton et al., 1977), theoretical investigations by Matthews (1978) and by Fukuyama and Kofman (1979) demonstrated that the presence of negative ions in the ionosphere leads to enhancement of the signal scattered to the incoherent-scatter radar receiver over that due to the electrons alone. The radar measurements thus lead to lower electron densities than were used in the preliminary studies. The reduction of measured N_e by introduction of the negative ion correction ranges from a small effect at 80 km altitude to a maximum factor of two where $\lambda = N_e/N_-$ becomes large at and below 60 km. This correction is taken into account in our analyses and is described in detail below.

The neutral chemistry model is similar to that described earlier (Gunton et al., 1977 and Reagan et al., 1978b) and has been improved with the latest reaction rate coefficients (De More, 1979).

The positive ion component of the simplified ion chemistry is also very similar to that of the earlier work. It includes five ions O_2^+, NO^+, O_4^+, NO^+W, and $H3O^+$. The latter two are lumped ions representing all of the species formed by clustering of NO^+, and the hydrated protons $H_3O^+ \cdot (H_2O)_n$, respectively. The ions other than O_2^+ and NO^+ are all given electron-ion recombination coefficients of $3 \times 10^{-6} cm^3 sec^{-1}$. In all of the cases considered, the predominant positive species are the hydrated protons. Although laboratory measurements (Leu et al., 1973) indicate that the rate depends on the degree of hydration, the use of a constant value in this simplified model appears to work well. Further discussion of the positive ion chemistry will be deferred to a complete report of the model to be prepared in the next phase of this work.

During the past year SRI International (R. Vondrak and J. Vickrey, private communication, 1979) have furnished to us electron density data at many more times for the 1972 event to complement the expanded data set for ion pair production developed at LMSC (Reagan et al., 1978b). It was, however, not possible within the scope of the current project, to make use of more than a small amount of the new data on electron density.

7.2 CORRECTION OF RADAR OBSERVATIONS OF ELECTRON DENSITY FOR THE PRESENCE OF NEGATIVE IONS

The SRI Chatanika incoherent-scatter radar measures a scattering cross section per unit volume.

$$\sigma_{total} = \frac{1}{2} N_{raw} R_e^2 \qquad (1)$$

where N_{raw} is the raw electron density and R_e is the electron radius.

The raw electron density is corrected in the absence of negative ions to actual electron density by use of the expression

$$N_e = \frac{N_{raw}}{2} (1+\alpha^2+Te/Ti) (1+\alpha^2) \quad (2)$$

in which $\alpha^2 = (\frac{2\Pi}{\lambda_R})^2 \lambda_D^2$, T_e is electron temperature, T_i is ion temperature, λ_R is the radar free space wavelength and λ_D is Debye length and no account is taken of the presence of negative ions. For the SRI radar $\alpha^2 = 13.9\ T_e/N_e$. Also for the D-region we may assume that T_e and T_i are both the same as the molecular temperature.

From the theory developed by Matthews (1978) and by Fukuyama and Kofman (1979) the correction equation for the raw electron density including the effect of negative ions may be written as

$$N_e = \frac{N_{raw}}{2} \quad \frac{1+2/\alpha^2(1+\lambda)}{1+1/\alpha^2(1+2\lambda)} \quad (3)$$

where λ is negative ion-electron ratio N_-/N_e. It is evident that to apply this correction the negative ion density or the ratio must be known.

As an aid in determining the negative ion density and the correct electron density the correction equation (3) has been solved together with the lumped parameter continuity equations

$$q = \alpha_D N_+ N_e + \alpha_I N_+ N_- \quad (N_+) \quad (4a)$$

$$aN_e = dN_- + \alpha_I N_+ N_- \quad (N_-) \quad (4b)$$

$$N_e = N_+ - N_- \quad (N_e) \quad (4c)$$

where all positive ions are lumped into N_+, negative ions are similarly lumped, q is the measured ion pair production rate, α_D is the effective electron-ion recombination coefficient, a is the attachment coefficient, d is the detachment coefficient, and α_I is the ion neutralization coefficient

The procedure is illustrated in Figure 7.1. The value of a for the altitude of the case can be calculated from the atmosphere density and temperature. The resulting set of pairs of values of α_D and d are compared with model results obtained as described above to find the best corrected value to be used for comparison with model calculations of the case.

7.3 NEGATIVE ION CHEMISTRY MODELING

The negative ion chemistry as presently known from laboratory measurements is very complex, involving many ions. A partial representation is given in Figure 7.2. The in situ observations of negative ions (Narcisi et al., 1972) as well as laboratory observations indicate that hydrates of many species, particularly of NO_3^-, are also very important. The rates of formation and removal of the hydrates are not yet very well known. The importance of the minor species O, $O_2(^1\Delta)$, O_3, CO_2, NO, NO_2 and, potentially, H_2O in negative ion chemistry can be readily seen. Detachment processes are very important to electron loss rates. Some of these are shown in Figure 7.2, but our analysis will subsequently suggest that others are probably missing.

The primary ion formation is the 3-body attachment to form O_2^-. Although other attachment channels are possible, for example to NO_2, they are generally minor and we do not include them. O_2^- is photodetached at a rate which is well known, and undergoes chemical associative detachment by O atoms. O_2^- is also detached by energy transferred in a collision with $O_2(^1\Delta)$. The complex ions formed from O_2^- and O^- are photodetached but the rates are generally not well known. Some negative ions are photodissociated, e.g., $CO_3^- + h\nu \rightarrow O^- + CO_2$ (Moseley et al., 1974). There are possible other significant reactions of this type which have not been discovered yet.

Because of this lack of information, particularly about hydration and about photoprocesses, in an effort to simplify the negative ion modeling problem we have developed a model consisting of four ions: O_2^-, X^-, Y^-, and Z^-. X^- represents a lumping of O_4^- and CO_4^-; Y^- represents O^-, O_3^-, and CO_3^-; and Z^- represents $O_2^-\cdot$ NO, NO_2^-, and NO_3^-. In X^-, CO_4^- is the dominant ion; in Y^-, CO_3^- is

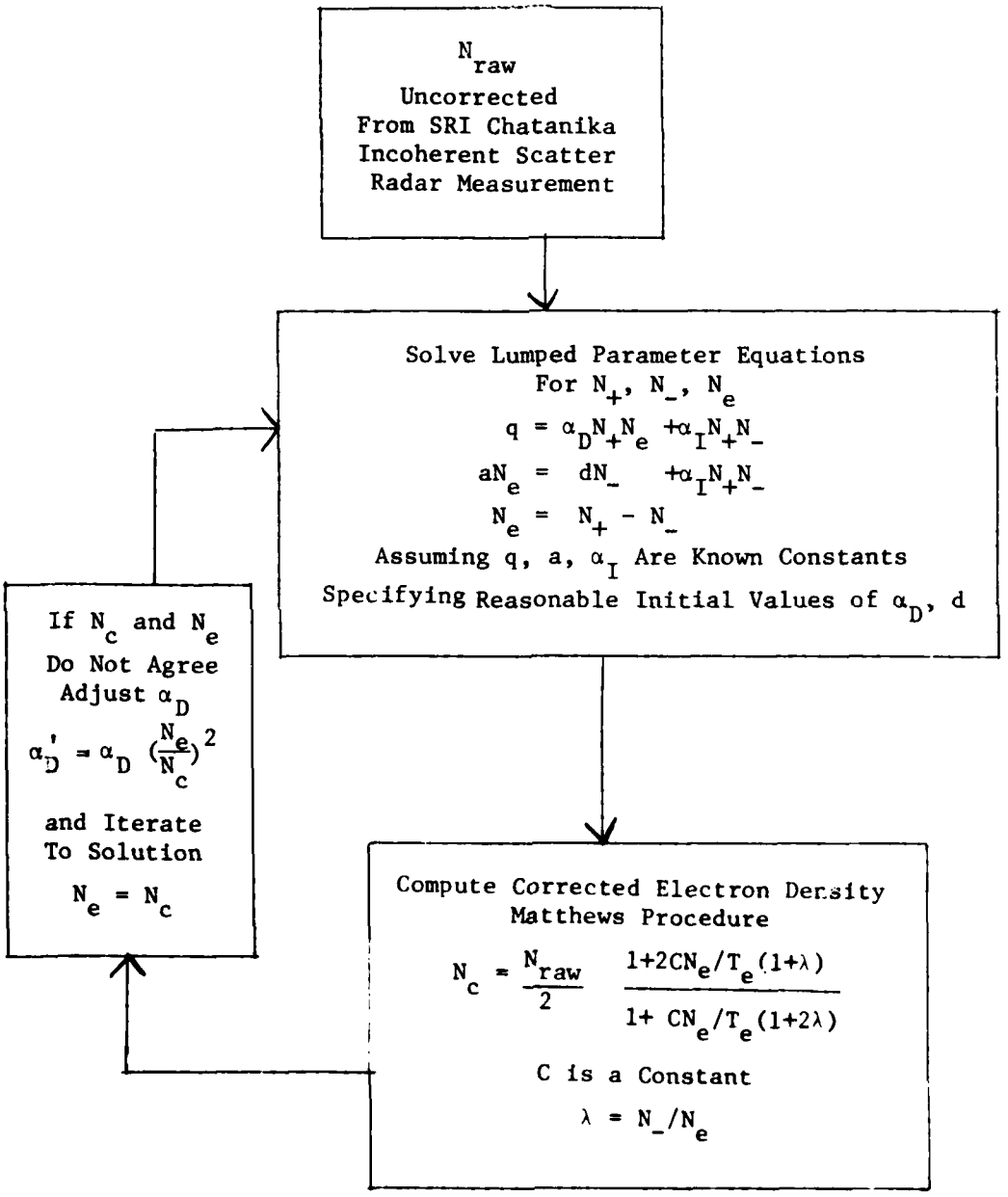

Figure 7.1. Procedure for correction of raw electron densities from radar measurement for the presence of negative ions.

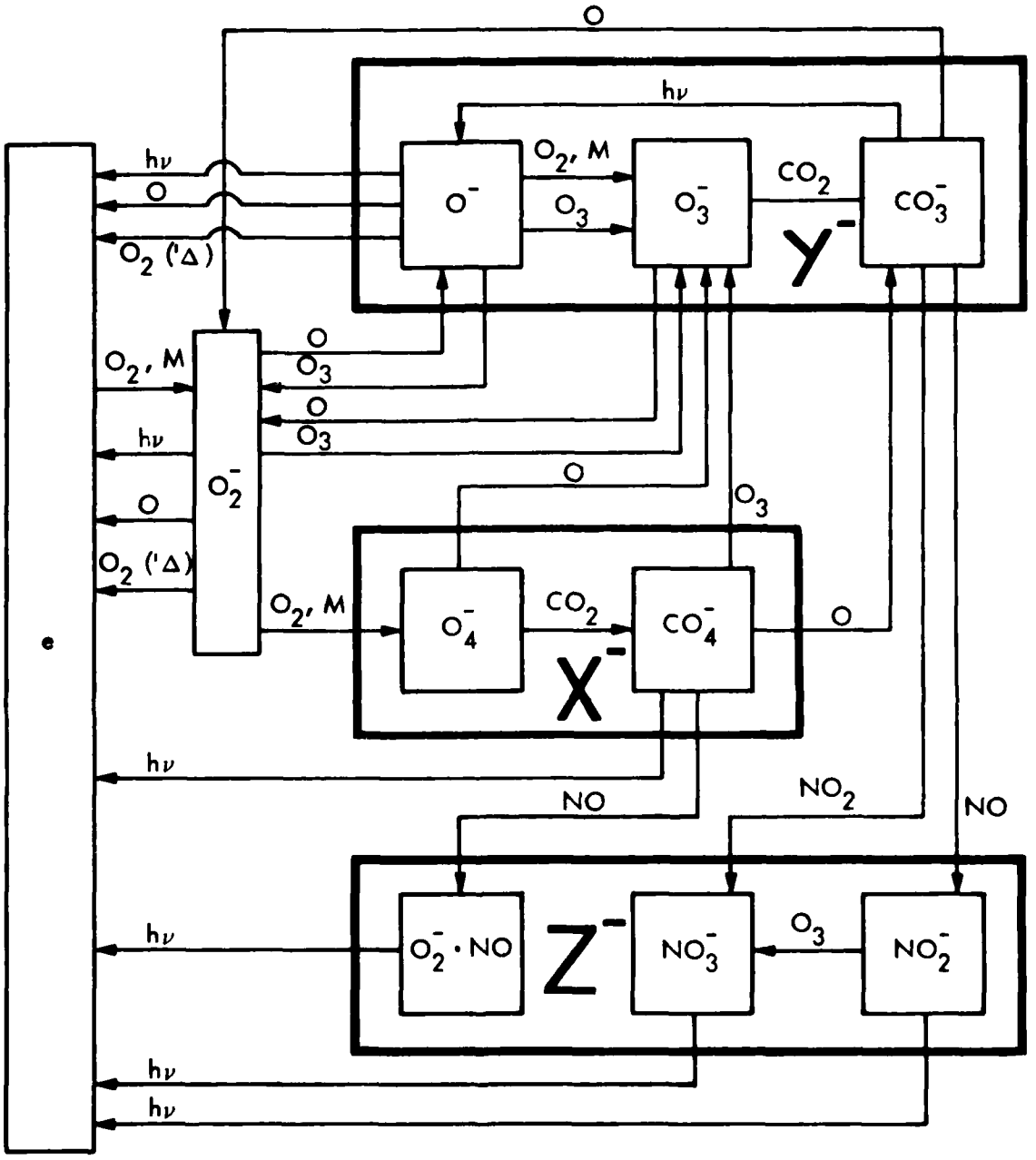

Figure 7.2. Schematic of part of the known negative ion reaction scheme showing the lumping together of ions used in the simplified scheme.

dominant although there may be significant small concentrations of O^-; and in Z^-, NO_3^- is usually dominant.

The simplified negative ion scheme is shown in Figure 7.3. The reactions are listed in Table 7.1 and each is assigned as far as possible a rate in the specified accuracy range of the laboratory measurement of the corresponding reaction as reported in the DNA Reaction Rate Handbook (1972) and its subsequent revisions.

Of course, all negative ions undergo neutralization with positive ions and these reactions are not included in the figures and in the table. The individual ion-ion neutralization rates are not very well known but recent work by Smith & Church (1977) indicates that most of the important positive-negative ion pairs found in the atmosphere have a rate of about 6×10^{-8} $cm^3 sec^{-1}$ and in the ion model this rate is assumed for all ions.

In determining the rates shown in Table 7.1 use has also been made of a more complex steady state ion model in which the negative ion portion is very similar to that of Swider et al (1978) and the positive ion portion includes the NO^+ hydration model of Reid (1977) and the standard reactions for hydration of O_2^+.

Certain rates in Table 7.1 must be regarded as empirically adjusted parameters, and these are for reactions 6, 12, 14, 15, 17, and 18. Adjustment of these parameters has been done by comparison of model results with the sets of corrected electron densities produced as described in Section 7.2. The result is a single set of empirically determined parameters used at all altitudes. The experimental data used includes all of the data from SPE72 at 28 points in time reported by Reagan and Watt (1976) at altitudes from 80 km to 50 km separated by 5 km. In addition the experimental data presented for PCA69 by Swider et al. (1978) at 70, 60, and 50 km have also been used. Emphasis, however, has been given to the SPE72 data obtained at five times when the satellite orbit passed close to the radar and to data at the lower altitudes 60 to 50 km. The reason for the latter emphasis is the hope that predictions made by this model will be useful at altitudes below 50 km where there is a lack of data for comparison.

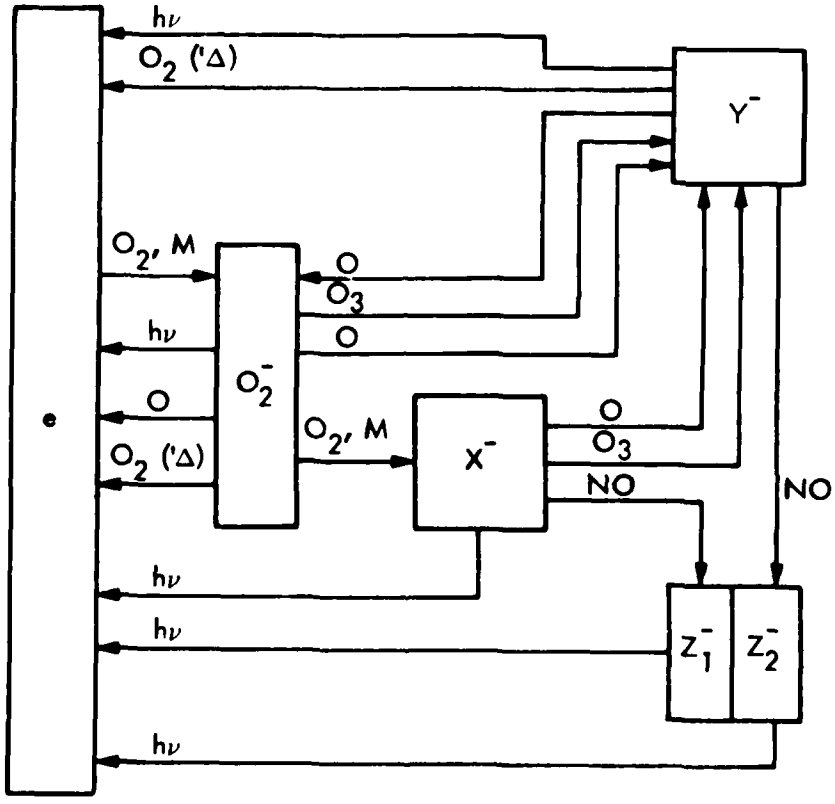

Figure 7.3. Schematic of simplified negative ion reaction model.

Table 7.1. Reactions and Rates of the Simplified Negative Ion Model

	Reaction		Rate*
1.	$e + O_2 + O_2$	$\rightarrow O_2^- + O_2$	1.2(-29)(300/T)EXP(-600T)
2.	$e + O_2 + N_2$	$\rightarrow O_2^- + N_2$	0.5(-31)
3.	$O_2^- + h\nu$	$\rightarrow e + O_2$	0.33
4.	$O_2^- + O$	$\rightarrow e + O_3$	3.(-10)
5.	$O_2^- + O_2(^1\Delta)$	$\rightarrow e + 2O_2$	2.(-10)
6.	$O_2^- + O_2 + M$	$\rightarrow X^-$	8.(-32)
7.	$O_2^- + O$	$\rightarrow Y^-$	3.(-10)
8.	$O_2^- + O_3$	$\rightarrow Y^-$	2.7(-10)
9.	$X^- + O$	$\rightarrow Y^-$	1.5(-10)
10.	$X^- + O_3$	$\rightarrow Y^-$	1.3(-10)
11.	$X^- + NO$	$\rightarrow Z_1^-$	4.8(-11)
12.	$X^- + h\nu$	$\rightarrow e$	0.2
13.	$Y^- + O$	$\rightarrow O_2^-$	1.3(-10)
14.	$Y^- + O_2(^1\Delta)$	$\rightarrow e$	1.2(-11)
15.	$Y^- + h\nu$	$\rightarrow e$	0.01
16.	$Y^- + NO$	$\rightarrow Z_2^-$	9.(-12)
17.	$Z_1^- + h\nu$	$\rightarrow e$	0.2
18.	$Z_2^- + h\nu$	$\rightarrow e$	0.03

*Units are sec^{-1}, $cm^3 sec^{-1}$, and $cm^6\ sec^{-1}$ for photon, 2-body and 3-body reactions, respectively.

In setting the rate of reaction 6, Table 7.1, it was considered desirable to reduce the value from the experimental measurement of 3.5×10^{-31} $cm^6 sec^{-1}$. Reaction 14 represents the detachment process $O^- + O_2(^1\Delta) \rightarrow E$ and is arbitrarily assigned a rate assuming that O^- is 4% of Y^-. Reaction 15 represents $O^- + h\nu \rightarrow E$. Reactions 12, 17, and 18 are given arbirary values since the actual values are unknown. It may be noted that Reaction 17 represents detachment from the $O_2^- \cdot NO$ component of Z^- and Reaction 18 is detachment from the NO_3^- component.

The atmospheric densities and temperatures are taken from CIRA 1972. The amounts of water vapor used in ppmv are 1.4, 2, 4, and 5 at 80, 70, 60, and 50 km for SPE72 and are 2, 2, and 5 at 70, 60, and 50 km for PCA69, respectively.

The ion pair production rates (Q) used for SPE72 are a new set computed from proton energy deposition and are reported by Reagan et al (1978b). These data consist essentially of one altitude profile per orbit and thus provide a much more detailed time coverage than the original data of Reagan and Watt (1976). The Q values for PCA69 were originally from Swider and Foley (1974) and have been adapted to the values at eight times given by Swider et al. (1978).

7.4 MODEL RESULTS

Typical results of the modeling are presented in Tables 7.2 and 7.3 and in Figures 7.3 and 7.4. In Table 7.2 the results for SPE72 are shown for altitudes of 80, 70, 60, and 50 km and for selected times. These times include at 70 and 60 km all of the five times at which the satellite passed overhead near the longitude of the radar. Also included in Table 7.2 for comparison are some results from the AFGL model for SPE72 at one of the times. The measured values shown have been corrected from the raw SRI Chatanika radar data for the presence of negative ions as described in Section 7.2. In a comparison of the results from the model described in this work and the electron densities derived from measurement it may be noted that at 80 km there is good agreement. Since at this altitude there is little contribution of attachment to the electron loss rate, this result indicates that the choice of the value 3×10^{-6} $cm^3 sec^{-1}$ for the electron-ion recombination coefficient is probably a reasonable one. On

Table 7.2. Measured and Calculated Electron Densities for SPE72

Altitude (km)	Date August	Local Time (AST)	Electron Density (cm^{-3})		
			Measured	Calculated (This Work)	AFGL Model*
80	4	0326	2.7(4)	2.8(4)	
		0508	3.2	3.5	6.7
		1706	2.9	2.8	
70	3	1916	1.4(4)	1.8(4)	
	4	0144	0.63	1.6	
		0326†	2.4	2.8	
		0508†	3.0	3.6	5.4
		1706†	2.0	2.3	
	5	0254†	1.0	1.2	
		1635†	0.84	1.1	
60	3	1916	3.1(4)	3.5(4)	
	4	0144	2.5	2.2	
		0326	1.3	1.4	
		0508	1.7	1.7	2.6
		1706	.81	.83	
		2331	.11	.03	
	5	0254	None		
		1635	2.9	3.5	
50	4	508	3.0	4.1	2.5

† The five times indicated are those for which the satellite passed overhead near the longitude of the radar.

* Swider at al. (1978)

Table 7.3. Measured and Calculated Electron Densities for PCA69

Altitude (km)	Date November	Local Time (CST)	Electron Density (cm^{-3})		
			Measured*	Calculated (This Work)	AFGL Model*
70	2	1510	1.8(4)	1.3(4)	1.8(4)
	3	0657	.23	.62	.7
		0730	.52	.62	.9
		0752	.65	.65	.9
		1254	.68	.59	.95
	4	1530	.37	.25	.3
		1638	.4	.24	.3
		1708	.24	.19	.24
60	2	1510	1.2(3)	.9(3)	.8(3)
	3	0657	.1	.49	.47
		0730	.2	1.9	1.3
		0752	.8	3.1	2.8
		1254	3.2	2.8	3.8
	4	1530	1.3	1.2	1.0
		1638	.7	.7	.4
		1708	.11	.1	.04
50	2	1510	1.5(3)	1.5(3)	.33(3)

* Swider et al. (1978)

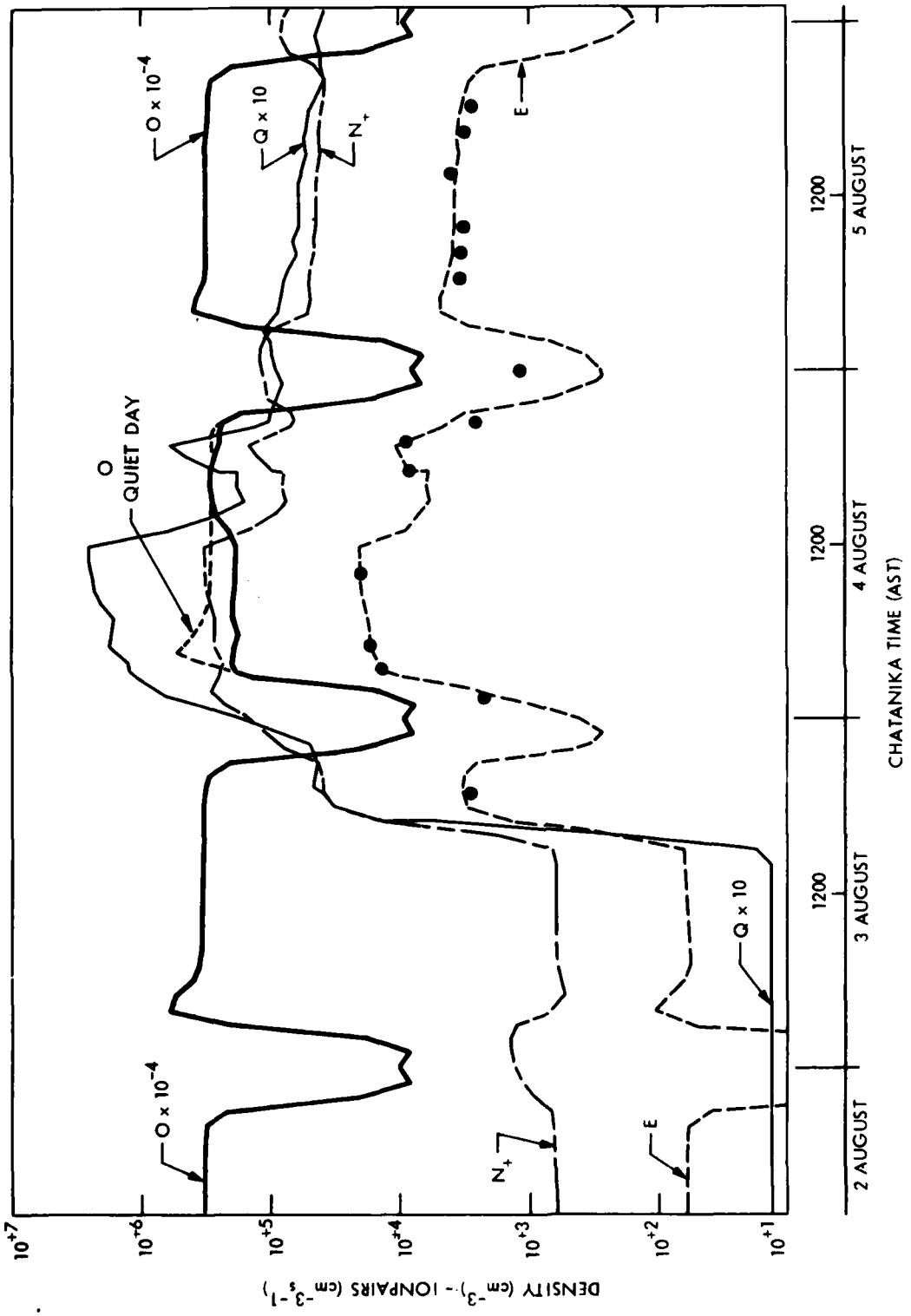

Figure 7.3. Plot of experimental ion pair production rate and calculated electron density, positive ion density, O atom density vs time at 60 km altitude during SPE72. The dots are the experimental electron density data from Chatanika radar measurements.

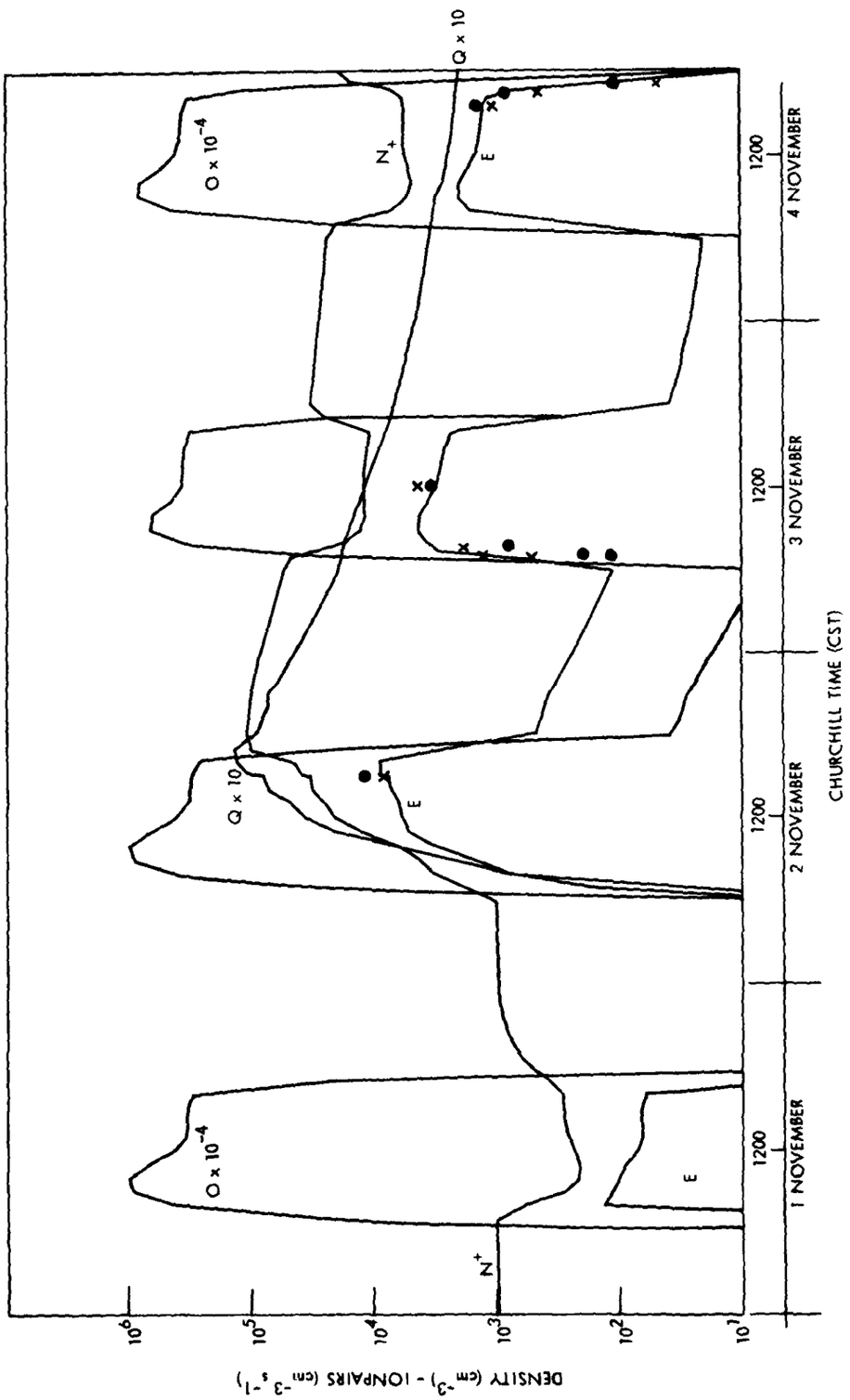

Figure 7.4. Plot of experimental ion pair production rate and calculated electron density, positive ion density, O atom density vs time at 60 km altitude during PCA69. The dots are experimental electron densities and the crosses are calculated electron densities from Swider et al. (1978).

the other hand at 70 km the model results are consistently larger than the measurements and this may indicate that the recombination coefficient should be larger than the value cited above which was assumed to apply to all ions other than O_2^+ and NO^+. At 60 km, agreement between model and measurement is good except at 2331 Alaska Standard Time (AST) on 4 Aug when the condition of deep twilight prevailed at this altitude. This reveals a probable fault in the model which will be investigated in future work. At 50 km, there is essentially only one available observation and model agreement with it is fairly good.

In Table 7.3, model results for PCA69 at 70, 60, and 50 km are compared with the measurements and AFGL model results reported by Swider et al. (1978). The first time of 1510 Central Standard Time (CST) on 2 November was near the peak of the event. The agreement of our model at this time with the only measured data at 50 km is quite good. In these PCA69 measurements there is demonstrated the long-known relative lag at sunrise of the rise of electron density. This may be seen in the data at 70 and at 60 km, at times of 0657 through 0752 CST on 3 November. There is an obvious asymmetry between sunrise and sunset which current models are unable to explain. They do agree reasonably well with the sunset results of 1530 through 1708 CST on 4 November. Figures 7.3 and 7.4 show the calculated diurnal behavior of N_e, N_+, Q, and O atom density at 60 km for several days before and during SPE72 and PCA69. The measurements of electron density and the AFGL model results are also shown.

In general, the agreement of our model with the two solar particle events of 1972 and 1969, differing in intensity, season, atmospheric densities, and temperatures, is good. Also, some preliminary calculations under ambient conditions show good agreement with observations made at 60 and 50 km. However, the latter problem will not be discussed further here it will be pursued in future work because of the importance of modeling ambient conditions for ELF propagation calculations.

Section 8

REFERENCES

Barr, R., The Effect of Sporadic-E on the Nocturnal Propagation of ELF Radio Waves, J. Atmos. Terrest. Phys., 39, 1379, 1977.

CIRA 1972 COSPAR International Reference Atmosphere 1972, North Holland Publishing Co., Amsterdam, Holland, 1972.

Davis, J. R., ELF Propagation Irregularities on Northern and Mid-Latitude Paths, in ELF-VLF Radio Wave Propagation, J. Holtet, Editor, D. Reidel Publ. Company, Dordrecht-Holland, pp. 263-277, 1974.

Davis, J. R., Localized Nighttime D-Region Disturbances and ELF Propagation, J. Atmos. Terrest. Phys., 38, 1309, 1976.

Davis, J. R. and W. O. Meyers, NRL Report 7924, Naval Research Laboratory, Washington, D.C., 1975.

DeMore, W. B., Ed., Chemical Kinetic and Photochemical Data for Use in Stratospheric Modeling, Evaluation Number 2, NASA Panel for Data Evaluation, JPL Publication 79-27, Jet Propulsion Laboratory, 15 April 1979.

DNA Reaction Rate Handbook, edited by M. H. Bortner and T. Baurer, DNA 1948H, Defense Nuclear Agency, March 1972.

Fukuyama, K. and W. Kofman, Incoherent Scattering of an Electromagnetic Wave in the Mesosphere: A Theoretical Consideration, Solar Terrestrial Environmental Research (Japan), V. 3, 1979 (in press).

Gunton, R. C., R. E. Meyerott, and J. B. Reagan, Ion and Neutral Chemistry of the D-Region During the Intense Solar Particle Event of August 1972, Final Report LMSC-D556351, Lockheed Palo Alto Research Laboratory, January, 1977.

Imhof, W. L., T. R. Larsen, J. B. Reagan, and E. E. Gaines, Analysis of Satellite Data on Precipitating Particles in Coordination with ELF Propagation Anomalies, LMSC-D502063, Lockheed Palo Alto Research Laboratory, Palo Alto, CA, 30 April 1976.

Imhof, W. L., T. R. Larsen, J. B. Reagan,and E. E. Gaines, Analysis of Satellite Data on Precipitating Particles in Coordination with ELF Propagation Anomalies, LMSC-D560323, Lockheed Palo Alto Research Laboratory, Palo Alto, CA, 30 June 1977.

Imhof, W. L., T. R. Larsen, E. E. Gaines, J. B. Reagan, R. C. Gunton, and R. E. Meyerott, Analysis of Satellite Data on Precipitating Particles in Coordination with ELF Propagation Anomalies, LMSC-D633266, Lockheed Palo Alto Research Laboratory, Palo Alto, CA, 30 November 1978.

Keneshea, T. J., and W. Swider, Formulation of diurnal D-region models using a photochemical computer code and current reaction rates, J. Atmos. Terrest. Phys., 34, 1607, 1972.

Larsen, T. R., Preliminary Discussion of ELF/VLF Propagation Data, in ELF-VLF Radio Wave Propagation, J. Holtet, ed., D. Reidel Publ. Company, Dordrecht, Holland, pp. 263-277, 1974a.

Larsen, T. R., ELF Noise Measurements, in ELF-VLF Radio Wave Propagation, J.Holtet, ed., D. Reidel Publ. Company, Dordrecht, Holland, pp. 285-289, 1974b.

Leu, M. T., R. Johnsen, and M. A. Bondi, Measurement of the recombination of electrons with $H_3O^+ \cdot (H_2O)_n$ – series ions, Phys.Rev., A7, 292, 1973.

Matthews, J. D., The Effect of Negative Ions on Collision-Dominated Thomson Scattering, J. Geophys. Res. 83, 505, 1978.

Moler, W., Letter to DNA - 28 April 1978.

Moseley, J. T., R. A. Bennet, and J. R. Peterson, Photodissociation of CO_3^-, Chem. Phys. Lett., 26, 288, 1974.

Narcisi, R. S., C. Sherman, C. R. Philbrick, D. M. Thomas, A. D. Bailey, L. E. Wlodyka, R. A. Wlodyka, D. Baker, and G. Frederico, Negative Ion composition of the D- and E-regions during a PCA, in Proceedings of COSPAR Symposium on Solar Particle Event of November 1969, J. C. Ulwick, ed., AFCRL-72-0474, p. 411, Air Force Cambridge Research Laboratories, Bedford, Mass, Aug. 1972.

Pappert, R. A., and W. F. Moler, Propagation Theory and Calculations at Lower (ELF) Extremely Low Frequencies, IEEE Trans. Comm., Vol. COM-22, No. 4, 438-451, April 1974.

Pappert, R. A. and L. R. Shockey: Ionospheric reflection and absorption properties of normal modes at ELF, Interim Report No. 772, Naval Ocean Systems Center, 15 September 1977.

Pappert, R. A., L. R. Shockey, Effects of Strong Local Sporadic E on ELF Propagation, NOSC TR 282, Naval Ocean Systems Center (NOSC), San Diego, 15 August 1978.

Reagan, J. B., and T. M. Watt, Simultaneous Satellite and Radar Studies of the D-Region Ionosphere During the Intense Solar Particle Events of August, 1972, J. Geophys. Res., 81, 4579, 1976.

Reagan, J. B., W. L. Imhof, E. E. Gaines, T. R. Larsen, J. R. Davis, and W. R. Moler, Effects of Precipitating Energetic Particles on an ELF Communication Link, Paper presented at the Symposium on the Effect of the Ionosphere on Space and Terrestrial Systems, sponsored by the Naval Research Laboratory and the Office of Naval Research, Arlington, Virginia, January, 1978a.

Reagan, J. B., R. W. Nightingale, R. E. Meyerott, R. C. Gunton, R. G. Johnson, J. E. Evans, and W. L. Imhof, Effects of the August 1972 Solar Particle Events on Stratospheric Ozone, LMSC-D630455, Lockheed Palo Alto Research Laboratory, Palo Alto, CA, October 1978b.

Reid, G., The Production of Water-Cluster Positive Ions in the Quiet Daytime D Region, Planet. Space Sci., 25, 275, 1977.

Smith, D., and M. J. Church, Ion-Ion Recombination Rates in the Earth's Atmosphere, Planet. Space Sci., 25, 433, 1977.

Swider, W., and C. I. Foley, D-region ionization rates for the 2 - 5 November 1969 PCA event as determined from satellite proton flux measurements, AFCRL-TR-74-0190, Air Force Cambridge Research Laboratory, Bedford, Mass., April 1974.

Swider W., Composite PCA '69 Study: Final Report, AFCRL-TR-75-0149, Air Force Cambridge Research Laboratory, Bedford, Mass., March 1975.

Swider, W., and C. I. Foley, Steady-State Multi-Ion Disturbed D-Region Model, AFGL-TR-78-0155, Air Force Geophysics Laboratory, Hanscom AFB, Mass., 15 June 1978.

Swider, W., T. J. Keneshea, and C. I. Foley, An SPE-Disturbed D-Region Model, Planet. Space Sci. 26, 883, 1978.

Ulwick, J. C., Effective recombination coefficients and lumped parameters in the D-region during solar particle events, p. 571; and Comparison of black brant rocket rocket measurements of charged particle densities during solar particle events, p. 395, in the Proceedings of COSPAR Symposium on Solar Particle Event of November 1969, AFCRL-72-0474, Air Force Cambridge Research Laboratories, Bedford, Mass., Aug 1972.

Voss, H., Private Communication, 1977.

Distribution List for Lockheed
ELF Propagation Anomalies

Annual Technical Report LMSC-D681778
NR 089-142 30 Jan 1980

Department of Defense

Director
Defense Advanced Research Projects Agency
1400 Wilson Boulevard
Arlington, Virginia 22209

1 cy ATTN: TIO
1 cy ATTN: STO
1 cy ATTN: NRMO

Director
Defense Communications Agency
8th Street and South Courthouse Road
Arlington, Virginia 22204

3 cys ATTN: MEECN Office

Defense Technical Information Center
Cameron Station
Alexandria, Virginia 22314

12 cys ATTN: TC

Director
Defense Nuclear Agency
Washington, D.C. 20305

1 cy ATTN: STTL
1 cy ATTN: DDST
3 cys ATTN: RAAE
1 cy ATTN: RAEV

Joint Chiefs of Staff
Department of Defense
Washington, D.C. 20301

1 cy ATTN: J-6

Director
National Security Agency
Fort George G. Meade, Maryland 20755

2 cys ATTN: Technical Library

Under Secretary of Defense (Research and Engineering)
Department of Defense
Washington, D.C. 20301

2 cys ATTN: DDS&SS

Department of Commerce

U. S. Department of Commerce
Office of Telecommunications
Institute for Telecommunication Sciences
National Telecommunications and Information
Administration
Boulder, Colorado 80303

2 cys ATTN: W. F. Utlaut

Department of the Army

Commander/Director
Atmospheric Sciences Laboratory
U. S. Army Electronics Command
White Sands Missile Range, New Mexico 88002

1 cy ATTN: DRSEL-BL-SY-S
F. E. Niles

Director
U. S. Army Ballistic Research Laboratories
Aberdeen Proving Grounds, Maryland 21005

1 cy ATTN: George E. Keller

Commander
U. S. Army Foreign Sciences and Technology Center
220 7th Street, N.E.
Charlottesville, Virginia 22901

1 cy ATTN: Robert Jones

Department of the Navy

Chief of Naval Operations
Department of the Navy
Washington, D.C. 20350

1 cy ATTN: NOP 985
1 cy ATTN: NOP 094H

Chief of Naval Research
Department of the Navy
800 North Quincy Street
Arlington, Virginia 22217

1 cy ATTN: Code 465, R. G. Joiner
1 cy ATTN: Code 427, H. Mullaney

Commander
Naval Electronic Systems Command
Department of the Navy
Washington, D.C. 20360

1 cy ATTN: PME-117
1 cy ATTN: PME-117T
1 cy ATTN: PME 117-21
1 cy ATTN: PME 117-21A
1 cy ATTN: PME 117-22

Director
Naval Ocean Systems Center
Electromagnetic Propagation Division
271 Catalina Boulevard
San Diego, California 92152

1 cy ATTN: Code 2200, W. F. Moler
1 cy ATTN: Code 2200, John Bickel

Director
Naval Research Laboratory
4555 Overlook Avenue, S.W.
Washington, D.C. 20375

1 cy ATTN: Code 7700, Timothy P. Coffey
1 cy ATTN: Code 7709, Wahab Ali
2 cys ATTN: Code 7750, John Davis
1 cy ATTN: Code 2627

Commander
Naval Surface Weapons Center (White Oak)
Silver Spring, Maryland 20910

1 cy ATTN: Technical Library

Office of Naval Research , Western Regional Office
1030 East Green Street
Pasadena, California 91106

1 cy

Department of the Air Force

Commander
Air Force Geophysical Laboratory, AFSC
L. G. Hanscom Air Force Base, Massachusetts 01731

1 cy ATTN: OPR,
1 cy ATTN: LKB, W. Swider
1 cy ATTN: LKB, K. Champion

Director
Air Force Technical Applications Center
Patrick Air Force Base, Florida 32920

1 cy ATTN: TD
1 cy ATTN: HQ 1035th TCHOG/TFS

Department of Defense Contractors

General Electric Company
TEMPO - Center for Advanced Studies
816 State Street
Santa Barbara, California 93102

1 cy ATTN: Warren S. Knapp
1 cy ATTN: DASIAC

Lockheed Missiles and Space Company
3251 Hanover Street
Palo Alto, California 94304

1 cy ATTN: J. B. Reagan
1 cy ATTN: W. Imhof
1 cy ATTN: Martin Walt

Mission Research Corporation
735 State Street
Santa Barbara, California 93101

1 cy ATTN: M. Scheibe
1 cy ATTN: D. Sowle

Pacific-Sierra Research Corporation
1456 Cloverfield Boulevard
Santa Monica, California 90404

1 cy ATTN: E. C. Field

Pennsylvania State University
Ionospheric Research Laboratory
College of Engineering
318 Electrical Engineering - East Wing
University Park, Pennsylvania 16802

1 cy ATTN: John S. Nisbet
1 cy ATTN: Les Hale
1 cy ATTN: A. J. Ferraro
1 cy ATTN: H. S. Lee

R&D Associates
4640 Admiralty Way
Marina Del Rey, California 90291

1 cy ATTN: R. Lelevier
1 cy ATTN: F. Gilmore
1 cy ATTN: R. Turco

The Rand Corporation
1700 Main Street
Santa Monica, California 90406

1 cy ATTN: Cullen Crain

Professor Chalmers F. Sechrist
155 Electrical Engineering Building
University of Illinois
Urbana, Illinois 61801

1 cy ATTN: C. Sechrist

Stanford Research Institute
333 Ravenswood Avenue
Menlo Park, California 94025

1 cy ATTN: Allen M. Peterson
1 cy ATTN: Ray L. Leadabrand

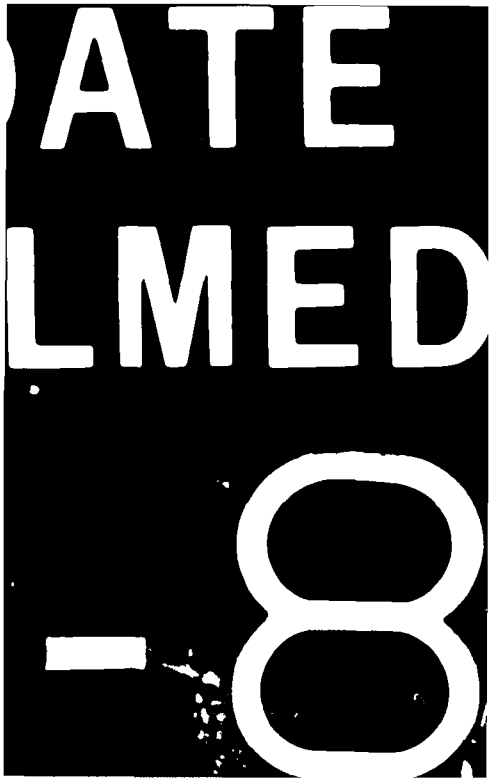
ATE
LMED
8